Computations on the Infra-red Spectra of Triatomic Molecules

by

Jeremy H. Schryber

A thesis submitted to

THE UNIVERSITY OF LONDON

for the degree of

DOCTOR OF PHILOSOPHY

University College London September 1997

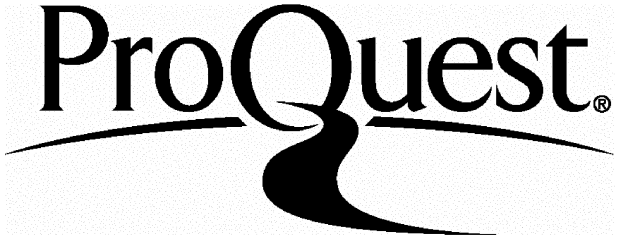

I dedicate this work in loving memory to Ali Morland and Tammy Silverman.

Abstract

"Computations on the Infra-red Spectra of Triatomic Molecules" is a write-up of two projects in the field of computational spectroscopy. The first is the calculation of the opacity of hot water vapour.

The water molecule is one of the most important absorbers in the *infra red* spectrum and it has been studied at length. Perhaps surprisingly, there is little reliable data on hot water (above $\sim$ 1000 K) available. The major source of experimental data is around twenty-five years old and is flawed. It is both inaccurate and imprecise. Another source for molecular data is the HITRAN database. The HITRAN data gives very accurate results for water at low temperatures but is unreliable at the higher temperatures encountered, for example, in the atmospheres of cool stars.

It was clear that the available data for hot water was somewhat lacking. Since there is interest in modelling cool stellar atmospheres it was necessary to calculate a more comprehensive list of molecular data. The results of those calculations are presented including a comparison with the previously available sources of data. Subsequent developments in this area and possible future work are discussed.

The second project is the calculation of an effective potential energy surface for the ground electronic state of nitrogen dioxide. Nitrogen dioxide has a somewhat unusual electronic structure which makes it a particularly interesting molecule. This also creates difficulties peculiar to nitrogen dioxide. Another reason for working on this molecule is that it is a significant atmospheric pollutant and absorber. There have been a number of attempts to determine an accurate ground state potential energy surface for nitrogen dioxide. These attempts are described and their deficiencies discussed. The method with which the new surface was determined is presented. Rovibrational calculations on the

surface are compared with observations and possible future work is considered.

Contents

List of Tables

List of Figures

Acknowledgements

I am a little wary of breaking with tradition in the first sentence of this thesis but I feel I must do so by thanking first and foremost my parents. Their help and support has been unwavering and unbounded during both the good times and the not so great. Without their backing and encouragement over the last few years, I would not have been able to perform the work presented herein.

Another person with a claim in that respect is my supervisor, Jonathan Tennyson. It has been his ideas, enthusiasm and direction that have propelled me while I have worked at UCL. I would also like to acknowledge the invaluable technical assisstance given to me by Oleg Polyansky for the work on NO_2.

I could not possibly thank all my friends and colleagues individually without making this section rather overlong. Thus, a general "Thank you" must suffice. However, I would like to thank, in particular, all who have shared Room A7 (my penthouse home from home) over the years. The list includes: Ruth Le Sueur, Nic Fulton, Serena Viti, Paul Dando and Rita Prosmiti amongst others. Their informative and entertaining(!) discussions elevated my quality of life at UCL hugely and they occasionally helped with my work too.

I would like to acknowledge the Engineering and Physical Sciences Research Council for supporting my work.

Chapter 1

Introduction

1.1 Introduction to Molecular Spectroscopy

Spectra, the absorption or emission of light at characteristic wavelengths, have long been known to provide accurate fingerprints of molecular species. Spectroscopy is routinely used for characterising samples even when in complex mixtures. It can also be used to help determine temperature and isotopic abundances. This is particularly useful in astronomy where molecular spectroscopy gives a unique handle on the conditions within, for example, molecular clouds and the atmospheres of planets and cool stars.

The detailed information contained in the spectrum of a molecule is a sensitive reflection of the underlying interactions within that molecule. The rotational transitions are a guide to the molecular geometry; vibrational transitions contain information about how the atoms within a molecule interact and thus can give detailed information about these interactions.

The nuclear motion within a molecule, or the interaction of the atoms, is described by a potential energy surface. These surfaces also contain information about reaction dy-

namics, transport properties and interactions in the liquid and solid states. For molecules larger than diatomics, it is not possible to directly invert spectroscopic data to obtain a potential surface. See below for more information on the construction of potential energy surfaces.

1.2 Motivation for molecular spectroscopic data

Spectra of polyatomic molecules are generally complicated sometimes containing thousands of lines. Assigning these spectra, i.e. determining the upper and lower states for each transition, can be difficult. This process can be greatly aided by calculations. Similarly, computed predictions of the locations of transitions can help the search for a particular species.

One important area for infra red spectroscopy is the modelling of the Earth's atmosphere particularly in relation to the Greenhouse effect. The opacity (the total absorption as a function of wavelength) of the atmosphere in the infra red region is critically important. The value of work towards computed opacities for atmospheric molecules is thus clear.

1.3 Need for, and construction of, potential energy surfaces

The Born-Oppenheimer approximation [1] proposes that due to the greatly differing masses of the nuclei and electrons, their motions can be considered separately. That is, nuclei move very much more slowly than electrons so it can be assumed that the electrons

instantaneously relax to any changes in position of the nuclei.

If the Born-Oppenheimer approximation is correct, it is possible to create an electronic potential surface (for a particular electronic state) and use this to solve the rovibrational properties of a molecule.

This potential may be created by *ab initio* calculations at a grid of points fitted to an appropriate functional form. It is also possible to create a potential surface by the more empirical method of determining the surface with reference to observed spectroscopic data. Such a surface may be refined by comparing computed results generated from it to observations. As the differences between the calculated and observed data are minimised, the surface is improved. For this to be possible, observed data must be available and understood. It should be noted that a surface constructed in this way may not be the Born-Oppenheimer surface. Any non-Born-Oppenheimer character of the molecule will be reflected in the observed data and thus the final surface will include that character.

1.4 Structure of this Thesis

Presented here are two separate projects. The first (see Chapter 2) is the calculation of the opacity of water up to high temperatures. The second (see Chapters 3 and 4) is the production of an effective ground electronic state potential energy surface for NO_2. What follows in this chapter is a general introduction to the field of molecular spectroscopy and to some of the theory behind the work presented later.

1.5 Methods of computing molecular spectra

Given a potential surface for a molecule, one must devise a method for calculating wave-functions and energy levels on it.

Low-lying states of small molecules are usually considered to undergo small-amplitude vibrations about some equilibrium geometry. Their rotations can be considered as those of a (near) rigid body. If interaction between vibrational and rotational motion is discounted in such a system, the vibrational wave-functions are the products of harmonic oscillators [2] and the rotational wave-functions are found by solving for a rigid rotor model [3].

This is of course inaccurate and can be improved by the use of perturbation theory [4, 5] This theory considers a system in terms of one with known solutions which has been slightly perturbed. Applied to the model of molecular vibrations, perturbation theory yields values for the derivatives of the potential at the molecule's equilibrium geometry. This gives a very good representation of the potential at equilibrium but not necessarily at any other arbitrary geometry.

1.5.1 The Hamiltonian Operator

In this section a discussion of the Hamiltonian operator for the nuclear motion (i.e. assuming the Born-Oppenheimer approximation) of a triatomic molecule in a generalised set of internal co-ordinates [6] is presented. These co-ordinates describe the relative motions of the nuclei. Each internal co-ordinate can be thought of as one of the system's degrees of freedom. Internal co-ordinates are generally considered to be advantageous as they lend themselves naturally to the distinction between rotations and vibrations. Certain computational advantages are also apparent.

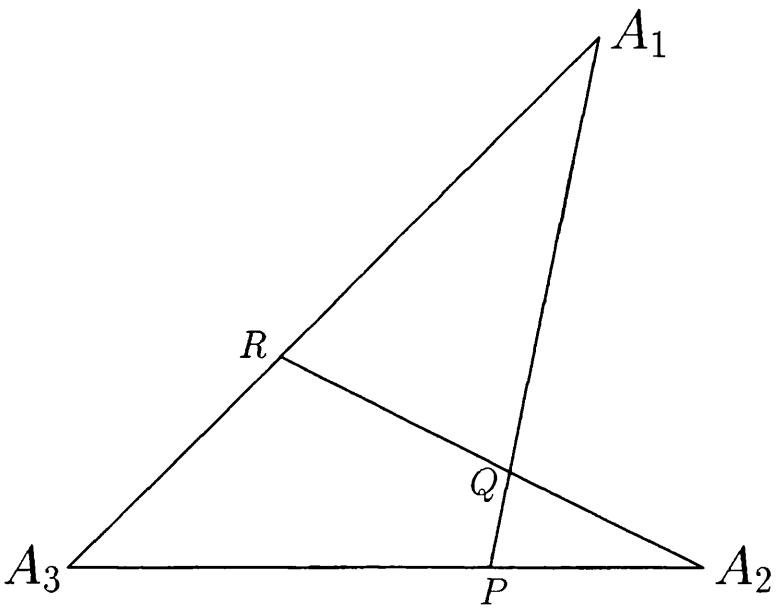

Figure 1.1: Triatomic co-ordinate system. A_i represents atom i. The co-ordinates in this work are given by $r_1 = A_2 - R$, $r_2 = A_1 - P$ and $\theta = A_1\hat{Q}A_2$.

For an N-body system, the number of internal co-ordinates is $3N - 6$. These are arrived at by taking the $3N$ absolute co-ordinates then subtracting 3 for translational motion of the whole system and then another three which are associated with the complete rotational motion of the system. Note that for a linear molecule one of its possible rotations is trivial so there are $3N - 5$ internal co-ordinates.

A highly generalised set of internal co-ordinates for a triatomic molecule is shown in figure 1.5.1. The system is defined in terms of two lengths and an included angle.

It is possible to define parameters g_1 and g_2 as [6]:

$$g_1 = \frac{A_3 - P}{A_3 - A_2}\ g_2 = \frac{A_3 - R}{A_3 - A_1}\ (0 \leq g_1, g_2 \leq 1) \tag{1.1}$$

Subsets of this generalised system include scattering co-ordinates where $g_1 = \frac{m_2}{m_2 - m_3}$, $g_2 = 0$; bondlength-bondangle co-ordinates where $g_1 = g_2 = 0$; and Radau co-ordinates where $g_1 = 1 - \frac{\alpha}{\alpha+\beta+\alpha\beta}$, $g_2 = 1 - \frac{\alpha}{1-\beta+\alpha\beta}$, where, $\alpha = (\frac{m_3}{m_1+m_2+m_3})^{1/2}$ and $\beta = \frac{m_2}{m_1+m_2}$.

For a three-body system the Hamiltonian, $\hat{H}$, is given by

$$\hat{H} = \frac{-(\hbar)^2}{2} \sum_{i=1}^{3} \frac{1}{m_i} \nabla_i^2(x_i) + V, \tag{1.2}$$

where $\nabla_i^2(x_i)$ is the Laplacian operating on the ith particle of mass i, and V represents the potential energy of the system. The axis frame in this form for the Hamiltonian can be regarded as arbitrary since the potential energy is invariant to translation or rotation.

It is necessary to remove the translational motion from this operator and also to transform the Hamiltonian after a particular axis embedding. Each time a new co-ordinate system or axis embedding is required, it is necessary to construct a new Hamiltonian for the system. A general method for deriving these Hamiltonians has been developed by Sutcliffe [7].

Unfortunately, the process of choosing internal co-ordinates and axis embedding introduces geometries into the Hamiltonian where it is badly behaved i.e. singular. For example these badly behaved geometries are often encountered when a molecule becomes linear. In this case, as mentioned above, the system has $3N - 5$ instead of $3N - 6$ vibrational modes. Thus special care is required for any bent molecule which samples linear geometries.

1.5.2 Variational Calculations

The variational principle [8, 9] allows one to construct and diagonalise a Hamiltonian matrix which is defined in terms of matrix elements linking some set of basis functions. It can then be shown that the better the representation offered by the set of basis functions, the lower the calculated energies will be [10]. Hence, in a series of calculations, as one enlarges and/or improves the basis set, the energies approach from above the 'exact' values.

For the ground state of a system consider:

$$\epsilon = \int \phi^* \hat{H} \phi dv, \tag{1.3}$$

where ϕ is an arbitrary, normalised wave-function which is single-valued, finite and continuous in the accessible space, and $\hat{H}$ is the full Hamiltonian operator of the system. If ϕ is set equal to the true ground state of the system, ψ_0, then

$$\int \psi_0^* \hat{H} \psi_0 dv = E_0. \tag{1.4}$$

Now, ϕ can be written as an expansion in the true wave-functions, ψ_n, of the system

$$\phi = \sum_{n=0}^{\infty} a_n \psi_n. \tag{1.5}$$

The true wave-functions form an orthonormal set and so we have the additional condition,

$$\sum_{n,m=0}^{\infty} a_n^* a_m = \delta_{mn}. \tag{1.6}$$

Substituting this into (1) gives

$$\epsilon = \sum_{n,m=0}^{\infty} a_n^* a_m \int \psi_n^* \hat{H} \psi_m dv. \tag{1.7}$$

Since the ψ_n are the true wave-functions of the system, we have,

$$\hat{H}\psi_n = E_n \psi_n \tag{1.8}$$

and

$$\epsilon = \sum_n a_n^* a_n E_n. \tag{1.9}$$

Subtracting $\sum_n a_n^* a_n E_0$ from each side of (7) and using

$$\sum_n a_n^* a_n E_0 = E_0 \sum_n a_n^* a_n = E_0 \tag{1.10}$$

leads to

$$\epsilon - E_0 = \sum_{n=0}^{\infty} a_n^* a_n (E_n - E_0). \tag{1.11}$$

The product $a_n^* a_n$ is either zero or positive. Thus, since E_0 corresponds to the energy of the lowest state of the system, E_n must be greater than or equal to E_0. Therefore it is true that

$$\epsilon \geq E_0. \tag{1.12}$$

So using this method it is possible to minimise ϵ thus achieving the closest possible approximation to E_0 for the original functions ϕ. This variational method can be extended to give a similar result for the energy of an excited state provided that the trial

function ϕ is made orthogonal to all the energy eigenfunctions corresponding to states having a lower energy than the level being considered.

Consider energy levels in ascending order: $E_0, E_1, E_2, \ldots$ and let the trial function, ϕ, be orthogonal to the energy eigenfunctions $\psi_n (n = 0, 1, \ldots i)$, i.e.

$$\langle \psi | \phi \rangle = 0, \quad n = 0, 1, \ldots i \tag{1.13}$$

Then if we expand ϕ in the orthonormal set $\{\psi_n\}$ as in equation 1.5, we have

$$a_n = \langle \psi | \phi \rangle = 0, \quad n = 0, 1, \ldots i \tag{1.14}$$

and $E(\phi)$ becomes

$$E(\phi) = \frac{\sum_{n=i+1} |a_n|^2 E_n}{\sum_{n=i+1} |a_n|^2} \tag{1.15}$$

so that

$$E_{i+1} \leq E(\phi) \tag{1.16}$$

As an example, suppose that the lowest energy eigenfunction, ψ_0, is known. Let ϕ be a trial function. Now, the function

$$\tilde{\phi} = \phi - \psi_0 \langle \psi_0 | \phi \rangle \tag{1.17}$$

is orthogonal to ψ_0 (i.e. $\left\langle \psi_0 | \tilde{\phi} \right\rangle = 0$) and can therefore be used to obtain an upper limit of E_1, the exact energy of the excited state.

In many practical situations the lower energy eigenfunctions $\psi_n (n = 0, 1, \ldots i)$ are not known exactly so only approximations of these functions are available. In this case the

orthogonality condition (equation 1.13) cannot be achieved exactly and thus equation 1.16 is violated. For example, suppose that the (normalised) function ϕ_0 is an approximation to the true ground state eigenfunction ψ_0. If ϕ_1 is a trial function orthogonal to ϕ_0 (i.e. $\langle\phi_0|\phi_1\rangle = 0$) it may be shown that

$$E_1 - \epsilon_0(E_1 - E_0) \leq E(\phi_1) \tag{1.18}$$

where ϵ_0 is the positive quantity given by

$$\epsilon_0 = 1 - |\langle\psi_0|\phi_0\rangle|^2 \tag{1.19}$$

Thus $E(\phi_1)$ does not provide a rigorous upper bound to E_1. However, if ϕ_0 is a good approximation to ψ_0 then ϵ_0 will be small and the violation of $E_1 \leq E(\phi_1)$ will be mild.

1.5.3 FBR

For triatomic molecules ro-vibrational energy levels are frequently found by using basis set expansions and the variational principle. Given an internal coordinate system, **Q**, and a Hamiltonian the next step in the variational approach is to choose basis functions to represent the motion of the nuclei. Vibrational motion can be expressed as products of suitable one-dimensional functions, $P(Q)$, so that the wavefunction of a vibrational state i can be written

$$\Psi_i(Q_1, Q_2, Q_3, \ldots) = \sum_{j,k,l,\ldots} c^i_{j,k,l,\ldots} P_j(Q_1) P_k(Q_2) P_l(Q_3) \ldots \tag{1.20}$$

where the expansion coefficients c^i are obtained by diagonalising the secular matrix constructed in terms of the basis functions. This method is known as the finite basis

representation (FBR). The term finite is used to stress that in practice it is necessary to truncate what should in principle be an infinite expansion.

Suitable basis functions include harmonic oscillators (Hermite polynomials), Morse oscillators (Laguerre polynomials) and related functions, and free rotor functions (Legendre polynomials). Harmonic [11] and Morse [12] oscillator functions contain parameters that can be optimised using the variational principle to obtain compact one-dimensional basis sets.

For a given basis set it is necessary to integrate over all coordinates to form the secular matrix. For an arbitrary potential function analytical evaluation may not be possible so this integration required numerical quadrature. A very satisfactory way of doing this is to note that all the basis functions mentioned above can be expressed in terms of orthogonal polynomials. The integrals can be evaluated numerically using the appropriate Gaussian quadrature scheme for each function [11, 12, 13].

Rotational motion is carried in these calculations by Wigner rotation matrices, $D^J_{k,M}(\alpha, \beta, \gamma)$. Unlike the vibrational basis functions, these form a finite set. I.e. For a given value of J it is necessary to include only the $2J + 1$ functions with $-J \leq k \leq +J$, where k is the projection of J on the molecular z axis. In practice the rotational parity can be used to separate this problem into ones of dimension $J = 1$ and J with $P = 0$ and $P = 1$ respectively. In this case the overall rotational parity is given by $(-1)^{J+P}$.

The coupled rotation-vibration problem is best solved in two steps [14, 15]. Firstly solve $J + 1$ vibrational problems, one for each value of $|k|$. The lowest solutions of these problems are selected as a basis for the fully coupled problem [15].

1.5.4 DVR

One problem with using the basis set method is that only a small proportion of the solutions obtained by diagonalising the secular matrix are of any significance. This means that basis set calculations perform poorly when a large number of energy levels are required.

An alternative is to use a finite-element method such as the discrete variable representation (DVR) [16, 17]. Although this method is not strictly variational it has strong links with basis set methods. This is because the formulation of the problem in a DVR first requires the construction of the secular matrix in terms of appropriate (polynomial) basis functions. This matrix is then transformed to a grid of points determined by the appropriate Gaussian quadrature scheme for each function. In the DVR it is possible to define hierarchy of problems which can be diagonalised and the lowest solutions selected and used to expand the next problem [18]. In this fashion final Hamiltonian matrices are constructed with a very high informational content — up to half the solutions of the final matrix may be physically significant [19].

The difference between FBR and DVR is clear. In the FBR the solutions are expressed as coefficients of basis functions; in the DVR the solutions are expressed as the amplitudes of approximate solutions at a well defined set of grid points. The DVR is isomorphic to an FBR of the same order and where matrix elements are evaluated using the appropriate quadrature on the DVR points.

The DVR method relies on successive diagonalisation and truncation in coordinate (or point) space. This technique is extremely effective in supplying very representative intermediate bases. Indeed, it can be shown to give the optimal hierachy of adiabatic basis sets [17].

The DVR has an additional advantage over FBR. By working in point space the method actually 'scans' the potential energy surface during the calculation and so provides the best possible basis all over the regions of interest on the surface. For complicated and strongly coupled surfaces this is very useful.

As implied by its name, the DVR is used to solve the nuclear motion problem in a point space rather than in the continuous function space of the FBR. The DVR is achieved by taking the Hamiltonian operator in the FBR and transforming it using a unitary similarity transformation matrix. The major advantage of the DVR is that one can successively construct and diagonalise reduced dimension Hamiltonian matrices, and use a contracted set of these intermediate solutions as a basis to solve the next higher dimension Hamiltonian. This results in a final Hamiltonian of much reduced size (compared to an equivalent FBR calculation) and of very high informational content. Another important (computational) advantage is that, to a very good approximation, the DVR theory makes the potential energy function totally diagonal in the DVR grid points.

Chapter 2

Computed infra red absorption properties of hot water vapour

2.1 Introduction

The water molecule is one of the most important absorbers in the *infra red* spectrum and it has been studied at length. Perhaps surprisingly, there is little reliable data on hot water (above $\sim$ 1000 K) available. Ludwig [20] provides one source with his measurements of the absorption of water between 1000 and 3000 K. Ludwig quoted values for absorption coefficients of water in frequency bins with a width of 25 cm^{-1}. Ludwig's data has been extensively used for constructing water band profiles, atmospheric modelling, laser modelling, flame models and the analysis of cool stellar atmospheres.

Jones *et al* [21] analysed the atmospheres of M dwarfs. These stars have relatively low effective temperatures ($<$ 4000 K) allowing the presence of molecular species. Water is the major absorber, other significant species being TiO, VO, FeH, and CH_4. Jones *et al* used Ludwig's data in their attempts to calculate accurate effective temperatures.

Alexander *et al* [22] and Plez *et al* [23] developed, using the opacity sampling method, a table of randomly distributed water lines derived from Ludwig's experimental data. This work was then used by Brett *et al* [24] in their models of M dwarfs but this treatment failed to reproduce the infrared spectra of these stars [25].

Yoshida *et al* [26] performed an analysis of radiative heat transfer in a nonisothermal and nonhomogeneous atmospheric boundary layer. Specifically they investigated the effect of aerosols which they considered to emit, absorb and scatter radiation energy. They investigated the effect of aerosol diameter and found that in some cases the effect of aerosols is strong. They used Ludwig as their source of water absorption data.

Fowler [27] worked on a method for powering rockets. His method involves the use of a ground based high-power laser to transmit energy to a rocket. This energy has to be absorbed by the rocket and imparted to the fuel. To do this, a seed molecule can be placed in the H_2 fuel creating a mix eg H_2O in H_2. The temperature dependence of the coupling molecule's absorption coefficient (at the laser's frequency, while immersed in H_2) is thus of interest. Fowler refers to Ludwig for "spectroscopic properties" of H_2O.

Sources of hot water data other than Ludwig are less useful. Phillips [28] used a Fourier-transform spectrometer to obtain transmission spectra for water vapour at 300-1000 K over a limited range of the *infra red* spectrum. The high resolution data were averaged over a 25 cm^{-1} "bandpass" and band-model parameters were then determined by means of a nonlinear least-squares fit. There are other examples of less comprehensive data [29, 30] and only earlier work by Ludwig et al [30] investigated high temperatures. All of these studies used a resolution no greater than 25 cm^{-1}.

The HITRAN database [31] is a frequently used source for molecular data. This contains 30,117 individually measured lines for H_2O, although it should be noted that

some of the intensities were calculated rather than measured. The HITRAN data should lead to very accurate absorption coefficients at 300 K (for which it is primarily designed) but the database contains too few high lying levels to be reliable at high temperature.

It was clear that the available data for hot water was somewhat lacking. Since we are interested in modelling cool stellar atmospheres it was necessary to calculate a more comprehensive line list. Use of this line list has shown that the very coarse resolution of Ludwig's results is a major problem.

2.2 Data

This section and the following one contain some more detailed information concerning the sources of the data used in this work.

Ludwig measured the absorption coefficients of water at high temperatures experimentally using a flame apparatus. This consisted of a series of flattened tubes manifolded together. Each alternate tube supplied oxygen and hydrogen which were ignited to form hot water vapour. A regulated blackbody source was positioned at one end of the flame with a monochromator opposite it at the other end. Ludwig quoted results for absorption coefficients at seven temperatures between 300 K and 3000 K. The range of frequencies covered was 0 – 9300 cm^{-1}. Critically, this range was broken down in to large "bins" with a width of 25 cm^{-1}. It is this low-resolution which is one of the main problems with using his data.

The high-resolution transmission molecular absorption database (HITRAN) is a compilation of spectroscopic data for important atmospheric molecules. We used the absorption data for $H_2^{16}O$ from the 1986 edition (which is essentially unchanged in the 1992 and 1996 editions) to compare to our calculated line list and Ludwig. The database contains

30,117 lines in which it quotes values for:

J' Ka' Kc' F' Sym' J'' Ka'' Kc'' F'' Sym'' and for the natural abundance weighted transition probabilities, $|R^2|$, in Debye^2 (for each transition frequency, ω).

To calculate the integrated absorption intensity, in cm^{-2} atm^{-1}, for each transition we used the expression:

$$I = C\frac{\omega g(2J'+1)}{Q}\left(\exp(\frac{-E''}{kT}) - \exp(\frac{-E'}{kT})\right) \mid R \mid^2 \qquad (2.1)$$

where Q is the partition function (see equation 2.2), ω is the transition frequency in cm^{-1} , g is the nuclear spin degeneracy factor and the constant of proportionality, C, has the value 11.152 for the particular combination of units and natural abundance of atomic isotopes used in HITRAN.

The HITRAN database should give very accurate absorption coefficients at around 300 K. However, the database does not contain enough high-lying rotational levels and hot bands to be a reliable source at much higher temperatures.

2.3 Calculation of the Line List

Due to the lack of comprehensive data on hot water absorption, it was necessary to calculate a line list. The primary motivation was the need for such data to study cool stellar atmospheres [32]. The line list of infrared water transitions was generated using first principles quantum mechanics. This list has been used to model the atmosphere of the cool M dwarf star VB10 [33]. When this model was compared to result calculated with Ludwig's absorption data, it was found to be significantly different. This difference was the motivation for a more detailed comparison between the line list and Ludwig, using the HITRAN data as a further comparison.

The water line list was calculated using first principles quantum mechanics to find the rotation-vibration energy levels, wave-functions and associated dipole transition strengths. The calculation was performed using the TRIATOM [34] program which finds exact variational solutions for a given potential (within the Born-Oppenheimer approximation) using an FBR procedure.

The calculations were performed on the best, at the time, water potential available [35] due to Jensen [36]. Transition intensities were found using the DIPOLE3 program [37, 38] and the dipole surfaces of Wattson and Rothman [39]. The potential energy and dipole surfaces were constructed by optimising *ab initio* surfaces to reproduce high resolution spectroscopic results.

Detailed comparison of *all* the observed vibrational band origins calculated with those calculated using Jensen's potential shows a standard deviation of 6.4 cm^{-1} [35]. However for the bands of interest here, the calculations reproduce the band origins with a standard deviation of only 0.9 cm^{-1}. For low lying rotational levels Jensen's potential reproduces the observed rotational term values with a standard deviation of only 0.14 cm^{-1} [35]; but calculations for high lying rotational states ($J \sim 20$) show errors as large as 10 cm^{-1} [40]. Comparisons of individual line-strengths with those tabulated on the HITRAN database have been performed by Wattson and Rothman [39] and Lynas Gray *et al* [37] who found that most of the strong transitions were reproduced within the 10% error quoted in HITRAN.

The initial line list ("MT" line list), reported by Miller *et al* [41] (who give details of the calculations) was extended by Allard *et al* [33]. It is this line list that we use in this work. The line list is based on calculations performed for rotational levels up to $J = 30$. Although convergence was good for states with $J \leq 20$ it deteriorated to about

10 cm^{-1} for states with $J = 30$. All levels up to 11,000 cm^{-1} above the ground state are included as well as many, but not all, higher ones. Transitions were calculated using only rigorous selection rules concerning angular momentum ($\Delta J = 0, \pm 1$) and parity [42]. 8.4×10^6 transitions were calculated and 6.2×10^6, with line strengths greater than 10^{-10} D^2 (Debye squared), were retained in the line list used here. In part this procedure was used to remove spurious ortho↔para transitions discussed below.

One of the problems with the line list is that the calculations do not distinguish between wave-functions of the ortho and para states ([43]) of water. This is due to technical reasons originating from the choice of coordinates in the TRIATOM program. We therefore weighted ortho and para transitions with a nuclear spin degeneracy factor of $g = 2$. Of course the weighting should be $g = 3$ for ortho states and $g = 1$ for para states but this approximation is reliable at high temperatures since most of the high-lying rotational levels occur in (nearly) degenerate ortho–para doublets.

At low temperatures this approximation is not so good. Therefore we identified the 25,894 transitions associated with the vibrational ground state (in rotational levels up to $J = 10$) and gave each of them their correct nuclear spin factor. Detailed comparison with HITRAN data at 300 K showed that this procedure greatly improved our predicted absorption parameters at 300 K and made little difference at 3000 K. A similar procedure (i.e. assigning nuclear spin statistics by hand to low-lying levels) was found to give reliable partition functions for H_3^+ [44].

2.4 Calculation of the Absorption Coefficients

In equation 2.1, Q is the partition function. The partition function used here was was calculated directly from the MT line list ro-vibrational energy levels by explicit summa-

tion

$$Q = \sum_{J,i}(2J+1)g_i \exp(\frac{-E_{J,i}}{kT}) \tag{2.2}$$

where i runs over all the computed levels with rotational quantum number J, J values considered ran from 0 to 30 and, for reasons discussed above, $g = 2$ for all levels which had not been identified as ortho ($g = 3$) or para ($g = 1$). This is obtained as a sum over all available calculated levels. Clearly it is necessary to truncate the sum so the values for Q are a lower limit. Convergence tests [45] suggest that the error is less than 1% even at 3000 K. Our values for Q are in good agreement with those from other sources including HITRAN.

However, this definition of the partition function differs from that generally used in astrophysical calculations [46, 47]. The discrepancy stems from a difference in the value used for the atomic nuclear spin for H. The tendency in astronomy is to use $Q(atomic) = 2I + 1$ where $I = 1/2$ for hydrogen, whereas amongst non-astronomers the use of $Q(atomic) = 1$ is often favoured. So this difference works through as a factor of $(2I + 1)^2 = 4$ for water (remembering that for ^{16}O, $I = 0$).

In order to compare our calculated absorption coefficients (and those calculated from HITRAN) with Ludwig's data, initially we binned our results by frequency into bins of 25 cm^{-1}. No consideration to line-shape was given in this process. Estimates of the Doppler and pressure broadening half widths (based on formulae from Phillips [28]) show that these effects are negligible for our purposes; the self-broadening Lorentz half width is never greater than 0.5 cm^{-1} for pressures up to 1 atmosphere.

A smaller bin size of 5 cm^{-1} was also used. This clearly showed up how Ludwig's data smears out much of the structure in absorption profile.

2.5 Results and Discussion

Over the frequency range considered, at 300 K, (25 cm^{-1} bins) all three data sets produce similar results for the absorption coefficients (see figure 2.1).

At 3000 K (25 cm^{-1} bins), see figure 2.2, the absence of high J lines and bands arising from vibrationally excited states, together with the limited number of bands covered causes serious gaps in the HITRAN absorption coefficients. Ludwig's absorption coefficients above 4000 cm^{-1} appear to be larger than the others. A discrepancy between the Ludwig results and other measurements of the bands at 1.4 μm and 1.1 μm has already been noted [48]. We also find a similar mismatch with these new calculations of the 1.9 μm band and suggest that Ludwig's results overestimate the absorption coefficient of water over the entire 1 – 2 μm region at higher temperatures. The only other, even older, absorption coefficients available for this region at high temperature, due to Ferriso *et al* [30], give results very similar to Ludwig's and will not be considered further here.

Displaying our results and those from HITRAN in 5 cm^{-1} bins shows the huge effect of Ludwig's coarse 25 cm^{-1} bins. They clearly result in extremely poor resolution data since much more structure can be seen from HITRAN and our calculated coefficients. Examining the pure rotation spectrum at 300 K illustrates this point well, see figure 2.3. Ludwig seems to give a reasonable average value but clearly loses a great deal of the structure.

The presence or absence of structure is very important for considering radiative transport properties such as the opacity of a stellar atmosphere. Photon escape through gaps in the water spectrum can be very important and this effect increases the importance of any other absorbers that might fill the gaps.

At 3000 K, figure 2.4 Ludwig's results are blue shifted by about 100 cm^{-1} although

the general shape and magnitude of the band are satisfactory. We can see at 3000 K the deficiencies of the HITRAN database. The absorption band is too small and is truncated.

Examination of the stretching overtone at around 7200 cm^{-1} shows up some more interesting features. At 300 K, (figure 2.5) the magnitude of the absorption band is approximately equal for each of the sources of data. However, on closer examination it can be seen that a peak in the Ludwig data at 7200 cm^{-1} coincides with a dip in the absorption given by HITRAN and our calculations on the MT line list. . At 3000 K (figure 2.6) Ludwig overestimates the absorption as noted earlier. The general absorption profile is similar to ours. Again we can see that HITRAN does not contain sufficient lines to produce accurate absorption coefficients at high temperature. The bend-stretch combination around 1.9 μm shows similar comparisons.

2.6 Conclusions and Subsequent Work

We have shown that the MT line list can be used to produce the absorption coefficients for water, particularly at high temperature. These coefficients have been compared to those of Ludwig [20], but can be used in a more flexible and realistic manner to allow for the many gaps that appear in the *infra red* spectra of a light molecule such as water. In addition, using standard formulae (for example those quoted by Phillips [28]) line profiles can be generated for a range of temperatures, pressures and compositions.

The MT line list was their first attempt at the comprehensive treatment of the rotation-vibration spectrum of a triatomic system. There is no doubt that the accuracy and extent of the line list can be improved. In particular, new and significantly more accurate potential energy surfaces for water are now available [40, 49, 50] and the new 3D DVR code [38] not only resolves the problem with the ortho-para nuclear spin

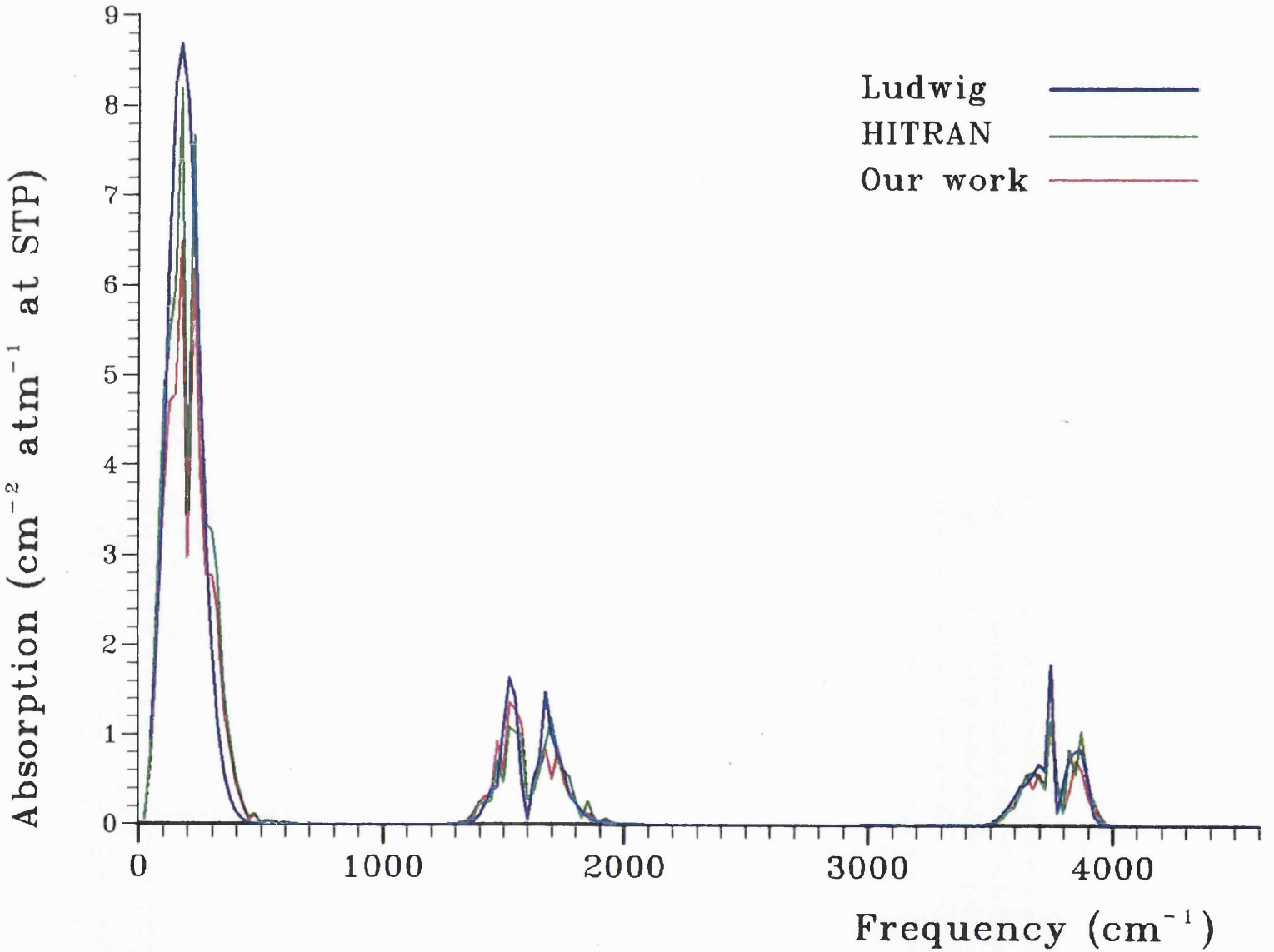

Figure 2.1: Absorption of light by water at 300 K, 25 cm^{-1} bins

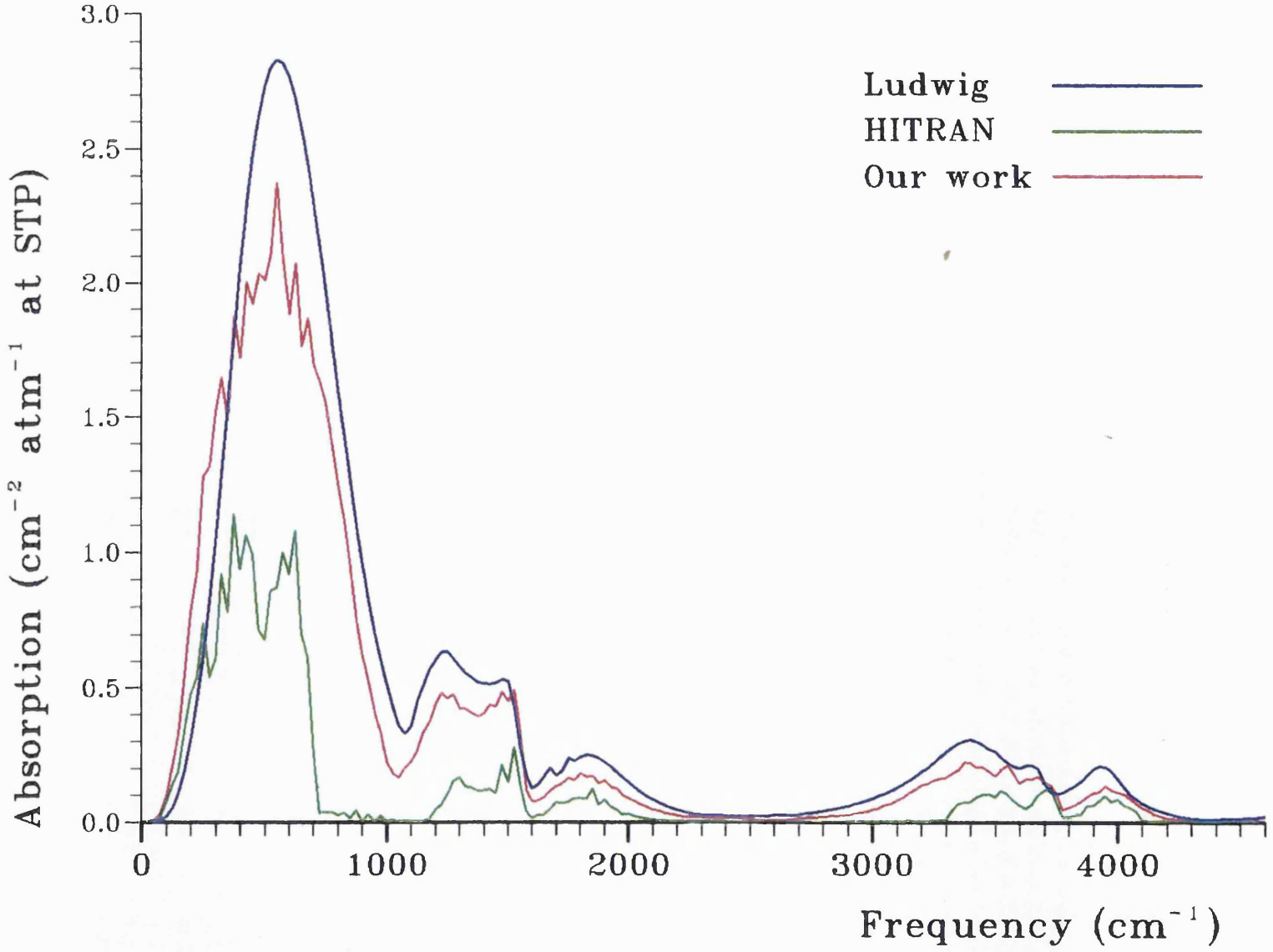

Figure 2.2: Absorption of light by water at 3000 K, 25 cm^{-1} bins

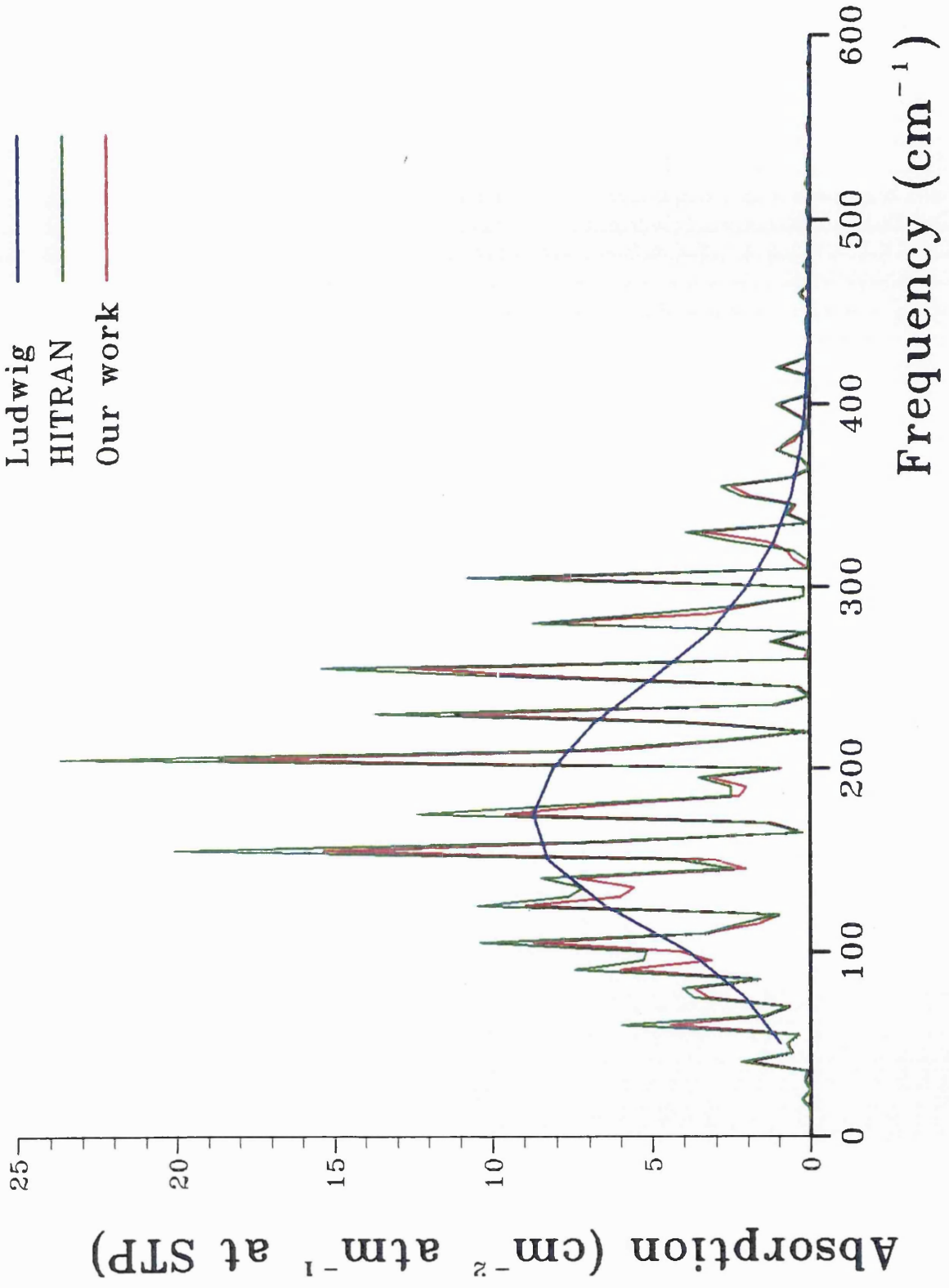

Figure 2.3: Absorption of light by water at 300 K, 5 cm^{-1} bins for HITRAN and this work

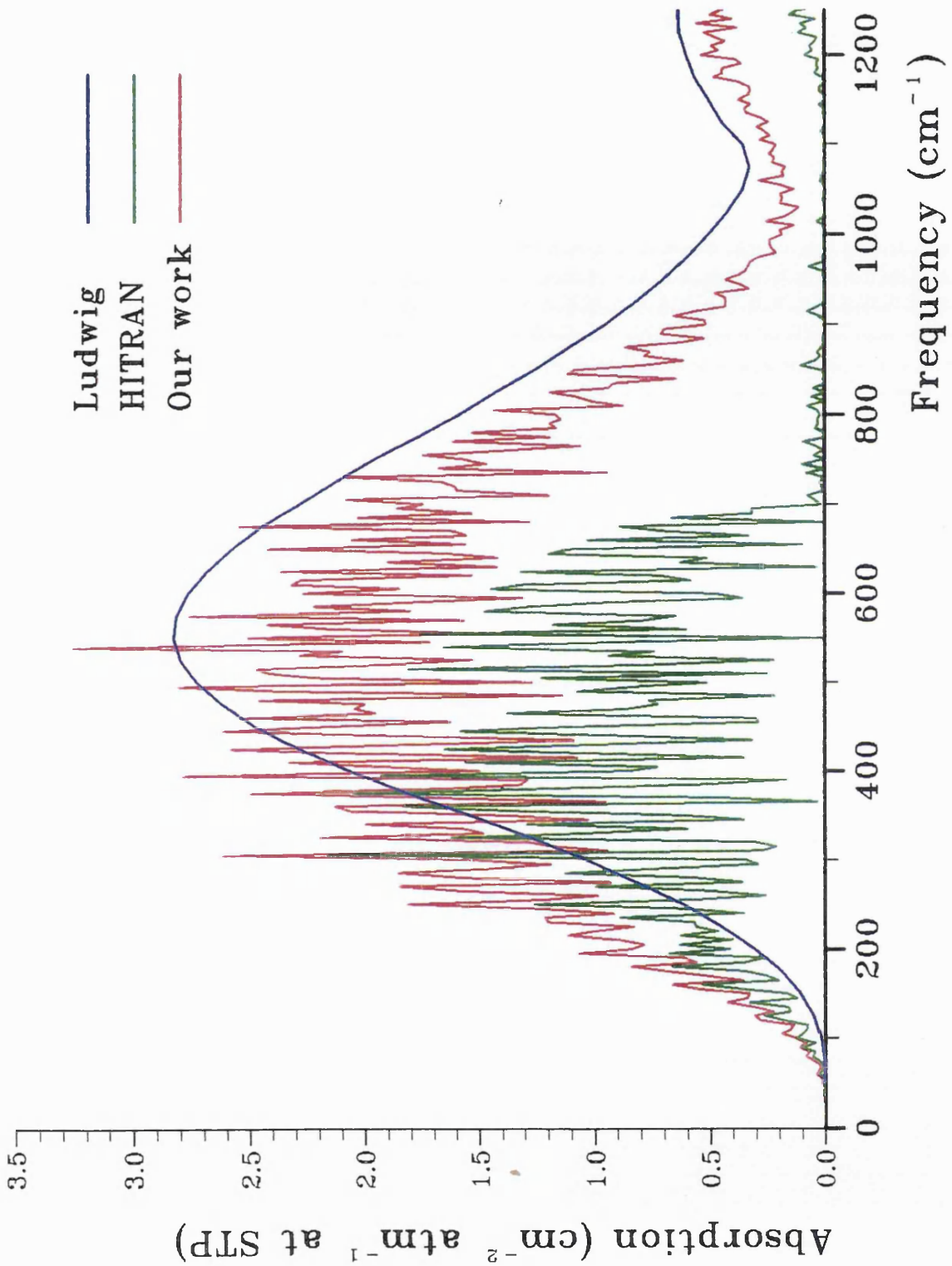

Figure 2.4: Absorption of light by water at 3000 K, 5 cm^{-1} bins for HITRAN and this work

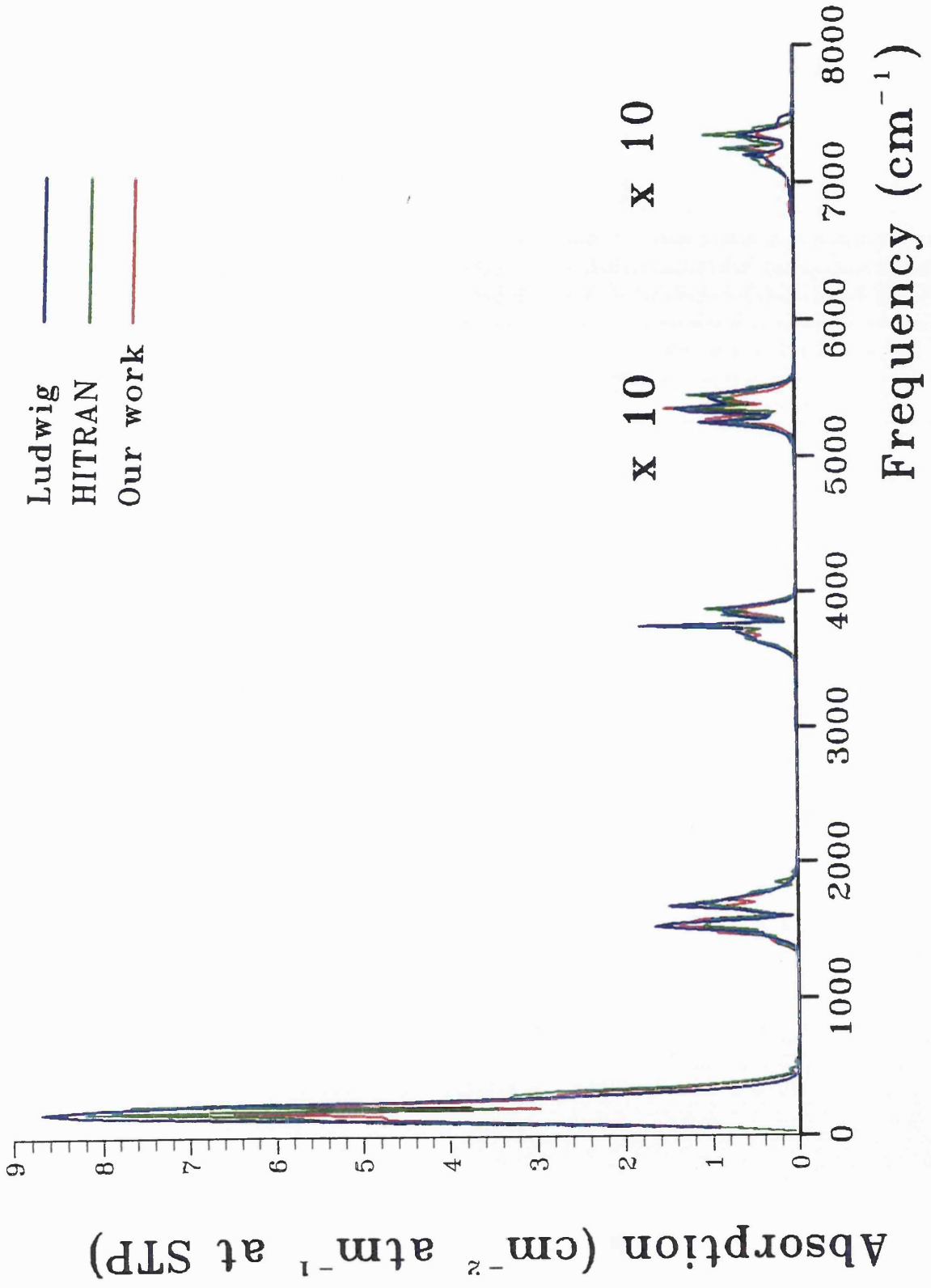

Figure 2.5: Absorption of light by water at 300 K, 25 cm^{-1} bins. The bands at $\sim$ 5100 and $\sim$ 7200 cm^{-1} have been magnified by a factor of 10 for clarity

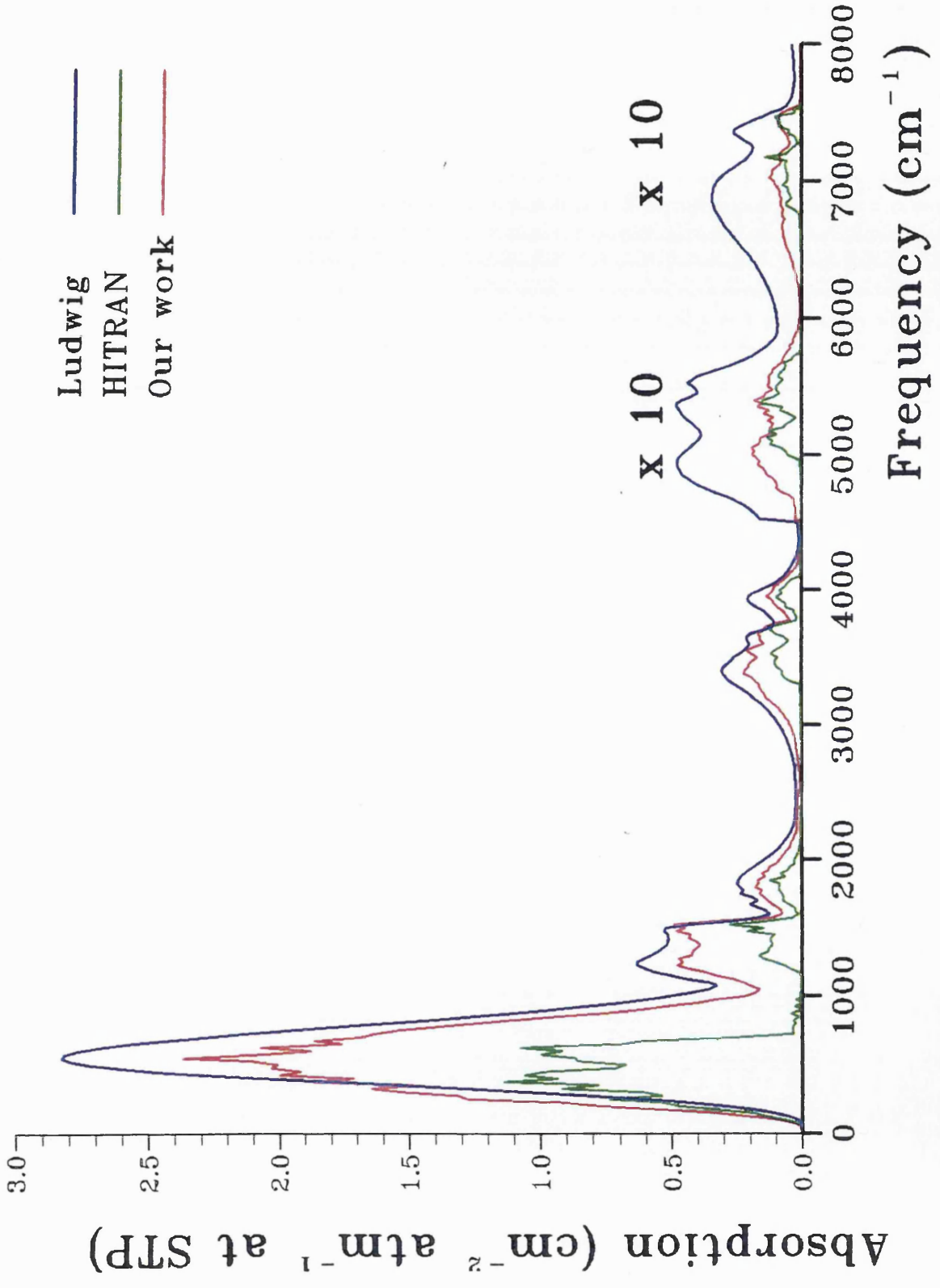

Figure 2.6: Absorption of light by water at 3000 K, 25 cm^{-1} bins. The bands at $\sim$ 5100 and $\sim$ 7200 cm^{-1} have been magnified by a factor of 10 for clarity

statistics discussed above, but also should allow the generation of reliable results for higher lying states. A new water linelist, taking advantage of these improvements, is currently being generated by Viti [51].

Subsequent to publication of this work, these results were commented on and used by other researchers. Jones *et al* [52] performed a comparison of observed and synthetic water spectra in a range of M dwarfs. The comparison shows good agreement. The effective temperatures found are similar to those of previous work. A definitive effective temperature scale was not determined. It is hoped that with the next generation water line list and a more complete understanding of molecular line broadening that this will be possible in the future.

Allard *et al* [33] presented results of model atmosphere calculations for cool M dwarfs. They compare the results of calculations performed using the MT line list and using Ludwig's experimental results. The calculations performed with the MT line list fit observations significantly better, thus demostrating the superiority of using the line list for modelling cool stellar atmospheres.

Subsequent to the work presented here, an extension of HITRAN was compiled: HITEMP [53, 54]. It is a mixture of measured an calculated transitions which includes some additional data for calculating opacities for higher temperatures. It has not yet been made generally available. There has been a new linelist published by Partridge and Schwenke [55] (PS). PS contains 300 million transitions and so offers a good database for high temperature computations.

Worden *et al* [56] took infrared spectrometer readings of wildfires in the western United States. In order to model the data that they had measured they required a background spectrum for hot water (amongst other molecules). They used data from

HITRAN for this purpose but found that they were unable to reproduce certain strong lines from their spectra. The work of Schryber *et al* [57] was used to highlight the fact that the HITRAN database was not sufficient for their requirements and that the initially unreproducible lines were from hot water.

Chapter 3

Critical Review of Potential Energy Surfaces for the X^2A_1 State of NO_2

3.1 Introduction

There are several reasons for attempting to create an accurate ground electronic state potential energy surface for NO_2. There is a full set of observed vibrational energy levels available [58]. The problem is interesting as quantum chaos sets in at higher energies [59, 60]. Also, a ground state PES is needed to study the problems involved with the coupling with the higher electronic state and to study the breakdown of the Born-Oppenheimer approximation. There is additional interest in NO_2 as it is an atmospherically important molecule, notably being involved in atmospheric ozone chemistry [61].

One of the reasons that the NO_2 molecules attracts considerable interest is its complex infra-red spectrum. This is caused to some degree by the crossing of its $^2A_1$ ground state and its $^2B_2$ excited states (see figure 3.1).

The $\tilde{X}^2A_1$ state has a conical intersection with the $\tilde{A}^2B_2$ state and forms a Renner pair

[43] with the $\tilde{B}^2B_1$ state at linear geometries. The $\tilde{A}^2B_2$ state has an energy relative to the ground state minimum of around 10,000 cm^{-1} at its equilibrium geometry, so clearly the potential surfaces described here are only an accurate representation of the ground state up to around that energy.

There have been a number of attempts to determine an accurate ground state potential energy surface for NO_2. These will be described in this chapter. Each of them is somewhat different from the others but all of them were suspect in one way or another. Problems with the surfaces include poor accuracy, spurious minima and a lack of comparison of calculated rotational data ($J > 0$) with observations.

3.2 Experimental data

In 1991, Delon and Jost [58] published the full set of 191 vibrational levels below 10,000 cm^{-1} and some levels up to 12,000 cm^{-1}. The method they employed was the Laser Induced Dispersed Fluorescence Spectroscopy of jet cooled NO_2. See next chapter for further details.

3.3 Hirsch, Buenker and Petrongolo

Hirsch, Buenker and Petrongolo (HBP) and co-workers have written a series of six papers on the vibronic structure of NO_2. Only the first four had been published at the outset of this work.

In paper 1 [63], they calculated potential surfaces for the two lowest $^2A'$ states of NO_2. They used the MRD-CI method to calculate the surfaces.

Paper 2 [62] describes the non-adiabatic coupling between the two previously calcu-

lated state and the construction of a diabatic representation for the states. The diabatic representation was determined by transforming the adiabatic CI wavefunctions.

HBP go on to produce both diabatic and adiabatic potential functions for the two lowest $^2A'$ states in part 3 [64] of their series. From these functions they find values for various features of the two states: equilibrium geometry, location of the crossing seam, excitation energy of the $\tilde{A}^2A'$ state and an estimate of the vibrational freqencies of the ground state.

In a Research Note [65], HBP considered the path from the $^2B_2$ stationary point to the minimum of the lowest $^2A'$ surface.

Part 4 [66] contains further calculations of the vibrational energy levels of the the electronic ground state of NO_2 in both the diabatic and adiabatic representations. HBP *et al* performed large-scale variational calculations and produced values for vibrational levels up to 18,000 cm^{-1} for the diabatic surface and compared levels up to 5,000 cm^{-1} of the adiabatic surface with experimental observations.

Part 5 [67] is a study of the nonadiabatic vibronic states of the $\tilde{X}^2A_1/\tilde{A}^2B_2$ conical intersection of NO_2. HBP *et al* computed 1500 nonadiabatic levels of the conical intersection up to 18,700 cm^{-1}.

The accuracy of HBP's calculated values for vibrational term values (computed nonadiabatic band energies) is very good for *ab initio* calculations. However, these type of calculations cannot produce spectroscopically accurate results for a molecule of this complexity. Indeed, the standard deviation for their calculated levels is around 18 cm^{-1} which is similar to the spacings between the levels. Many levels are tens of wavenumbers from the observed values. This resulted in HBP having difficulty in unambiguously matching calculated and observed levels. Note that the chaotic nature of the system can make

quantum number assignments somewhat arbitrary for the higher excited states.

3.4 Tashkun and Jensen

The first attempt to produce a spectroscopic potential for this system was made by Tashkun and Jensen [68]. TJ employed the MORBID [69] (Morse Oscillator Rigid Bender Internal Dynamics) computer program which approximates the kinetic energy term of the Hamiltonian. They used MORBID to refine the potential energy function for the $\tilde{X}^2A_1$ ground state of NO_2. They optimized an analytical representation of the potential function using data due to Delon and Jost. They considered the ground state surface to be independent of the any excited states. As they acknowledged this is not the case. At higher energies the interaction with the excited states will influence the energy level structure of the ground state.

The potential energy function used by TJ was originally given by Jensen [36]. This form was chosen as MORBID evaluates integrals exactly (analytically). All subsequent fits (see table 3.1) have also used this form:

$$V(\Delta r_1, \Delta r_3, \bar{\rho}) = V_0(\bar{\rho}) + \sum_j F_j(\bar{\rho}) y_j + \sum_{j \le k} F_{jk}(\bar{\rho}) y_j y_k + \sum_{j \le k \le m} F_{jkm}(\bar{\rho}) y_j y_k y_m + \sum_{j \le k \le m \le n} F_{jkmn}(\bar{\rho}) y_j y_k y_m y_n, \tag{3.1}$$

where all of the indices j, k, m, and n assume the values 1 or 3. The quantity y_j in Eq. (3.1) is given by

$$y_j = 1 - \exp(-a_j \Delta r_j) \tag{3.2}$$

where the a_j are molecular constants and $\Delta r_j = r_j - r_j^e$, $j = 1$ or 3, is defined as a displacement from the equilibrium value r_j^e of the distance r_j between the "outer" nucleus $j = 1$ or 3 and the "center" nucleus 2. The quantity $\bar{\rho}$ is the instantaneous value

of the bond angle supplement The $F_{jkm...}$ expansion coefficients of Eq. (3.1) are functions of $\bar{\rho}$ and defined as

$$F_j(\bar{\rho}) = \sum_{i=1}^{4} f_j^{(i)}(\cos\rho_e - \cos\bar{\rho})^i, \tag{3.3}$$

and

$$F_{jk...}(\bar{\rho}) = f_{jk...}^{(0)} + \sum_{i=1}^{N} f_{jk...}^{(i)}(\cos\rho_e - \cos\bar{\rho})^i \tag{3.4}$$

where ρ_e is the equilibrium value of $\bar{\rho}$ and the $f_{jk...}^{(i)}$ are expansion coefficients. The function $F_{jk}(\bar{\rho})$ has N=3, $F_{jkl}(\bar{\rho})$ has N=2, and $F_{jklm}(\bar{\rho})$ has N=1. The function $V_0(\bar{\rho})$ is the potential energy for the molecule bending with bond lengths fixed at their equilibrium values, and here we parameterize it as

$$V_0(\bar{\rho}) = \sum_{i=2}^{8} f_0^{(i)}(\cos\rho_e - \cos\bar{\rho})^i. \tag{3.5}$$

where the $f_0^{(i)}$ are expansion coefficients.

TJ used observations by Delon and Jost [58] to optimise their potential function. In their fit, TJ included levels only up to 9,500 cm^{-1} due to the possible perturbation of the ground state by its conical intersecton with the $\tilde{A}^2B_2$ state. For the same reason they gave the levels between 9,000 cm^{-1} and 9,500 cm^{-1} a much lower weighting.

In order to determine the equilibrium geometry, TJ supplemented the vibrational term values of Delon and Jost with a small number of rotational levels (computed by Kozin [70]). These levels were Pauli-allowed states with $N \leq 5$ in the vibrational ground state and the ν_1, ν_2, ν_3 and $2\nu_1$ states. Since MORBID does not account for spin-rotation interactions and hyperfine effects, it was necessary to calculate the "deperturbed" rotational spacings for NO_2 as the eigenvalues of a standard asymmetric rotor Hamiltonian.

The input data were reproduced with an RMS deviation of 0.2984 cm^{-1} for the rotational data and 2.20 cm^{-1} for the vibrational spacings. Note that the approximation of the MORBID kinetic operator introduces further systematic errors on top of this [35].

The TJ potential gives a reasonable description of the potential surface for NO_2 near the minimum. However, as can be seen from figure 3.2, it has spurious minima or "holes" away from the true minimum which is located at $\sim$ 2.2 Bohr and $\sim$ 2.3 radians. Note the large hole at short bond-lengths and bond-angles and the more serious hole at $\sim$ 1.8 Bohr and $\sim$ 3.0 radians. TJ suggest that this problem is not severe as the holes have a sufficiently high barrier to them (100,000 cm^{-1}) and that they can be removed by adding walls to the potential. This, however is somewhat artificial and leaves the potential function with discontinuities. These discontinuities gave us problems in using the potential in our codes, in particular with the Gaussian quadrature, when trying to calculate rovibrational energies. Leaving holes in a potential causes even greater problems.

3.5 Xie and Yan

The TJ potential was refined by Xie and Yan (XY) [71] contemporaneously to the work presented in this thesis. They used a variational method employing the exact vibrational Hamiltonian to calculate NO_2 energy levels. They fit their results to the 142 levels below 9,000 cm^{-1} using the Delon and Jost data. They optimized parameters for the potential function by minimizing a weighted least squares function:

$$F = \sum_n (w_n (E_n^{(obs)} - E_n^{(cal)}))^2, \tag{3.6}$$

This sum runs over the energy levels to be fitted. $E_n^{(obs)}$ are the observed values, $E_n^{(cal)}$ are the calculated values and w_n is the weighting function $1/E_n^{(obs)}$.

The derivatives of the calculated energies with respect to the potential parameters,

$\partial E_n/\partial p$, can be calculated by using the Hellmann-Feynman theorum (see Section 4.3.1):

$$\frac{\partial E_n}{\partial p} = \left\langle \Psi_n \left| \frac{\partial V}{\partial p} \right| \Psi_n \right\rangle, \tag{3.7}$$

where $\partial V/\partial p$ is the derivative of the potential with respect to a parameter and Ψ_n are the wavefunctions of the energy levels.

The result of this weighted least squares fit was a reduction in the standard deviation from 14.28 cm^{-1} to 2.08 cm^{-1}.

The final potential still contained holes. We attempted to test XY's surface but were unable to perform sensible variational calculations on it as published because of the presence of two separate holes. The less serious hole occurs when one bondlength is compressed below 1.3 Bohr. A more serious and extensive hole occurs in the symmetric stretch; its closest approach to equilibrium being where $r \sim 2.00$ Bohr $\theta \sim 2.0$ radians. Figure 3.3 shows the XY potential in the asymmetric stretch and illustrates the former of these holes. The more serious hole is clearly shown in a picture of the symmetric stretch (figure 3.4). We removed the effects of these minima by flattening the potential over the regions where they occurred. That is, in the regions where holes were evident we gave the potential the same value as that near top of the barrier into the holes.

XY did not use any rotational data in their fit nor did they quote any rotational data in their paper. A previous water potential due to XY [72] gave very poor results for rotations as shown by Polyansky and Tennyson (see Schryber *et al* [73]). This suggested that their NO_2 potential might also reproduce rotational levels poorly. It is dangerous to produce a potential energy function without reference to rotational data. It can lead to the incorpration of an inaccurate equilibrium geometry and thus an unphysical potential from which it it impossible to calculate reliable rotational data. In fact XY's potential

reproduces rotational term values reliably (see table 3.2 for a selection of rotational results using XY's potential).

3.6 Vilanove and Jacon

Vilanove and Jacon (VJ) [74] achieved a modest improvement of the TJ potential. They used a DVR method to calculate the energy levels of the electronic ground state of NO_2 up to 7,000 cm^{-1}. Their potential is not terribly accurate with a standard deviation of 9.8 cm^{-1} for a group of 78 levels. It also suffers from the same problem of having holes as does the TJ potential. See figure 3.5 for an illustration of this potential. Note that one of the potential parameters that they altered changes the equilibrium geometry. Thus we expect that the potential would give very poor rotational results. However, as we were unable to perform sensible nuclear motion calculations on this potential, we could not test this.

3.7 Conclusions

It is notable that although TJ used rotational data to help them determine their potential, all the subsequent spectroscopic determinations of the potential considered only vibrational term values. In view of the experience with water discussed above, such an approach must be viewed with caution. In particular, VJ chose to vary the parameter $f_1^{(0)}$ which TJ had fixed as zero. $f_1^{(0)}$ fixes the first derivative of the potential with respect to stretching coordinates at the expansion point. Resetting from zero has the effect of shifting the equilibrium geometry of the potential. Performing such a shift without reference to rotational data must be regarded as particularly dangerous. The need for a

new potential is clear as the others available each have their flaws.

Parameter	TJ	XY	VJ	This work
$f_0^{(2)}$	78903	78904.36	79528	78259.20740
$f_0^{(3)}$	−88508	−88177.07	−88508	−107129.99582
$f_0^{(4)}$	220230	217879.76	220230	225437.38541
$f_1^{(0)}$	0	0	−30	0
$f_1^{(1)}$	−9174	−9096.57	−11174	−9514.44438
$f_1^{(2)}$	−58601	−56772.84	−58601	−33493.10799
$f_1^{(3)}$	6626	18552.63	6626	−3080.26035
$f_1^{(4)}$	134673	118263.42	134673	0
$f_{11}^{(0)}$	26978	26964.43	26978	27019.00973
$f_{11}^{(1)}$	0	0	0	16052.75505
$f_{11}^{(2)}$	0	0	0	652.42584
$f_{11}^{(3)}$	184828	168337.50	184828	0
$f_{13}^{(0)}$	8927	8852.32	8927	9106.89156
$f_{13}^{(1)}$	29335	21809.35	29335	1094.98984
$f_{13}^{(2)}$	0	0	0	7446.65832
$f_{13}^{(3)}$	−425168	−462164.45	−425168	0
$f_{111}^{(1)}$	9550	7252.81	9550	0
$f_{113}^{(0)}$	0	0	0	−410.29378
$f_{113}^{(1)}$	3762	−593.46	3762	−1567.88852
$f_{113}^{(2)}$	213811	182066.42	213811	0
$f_{1113}^{(0)}$	1854	4059.13	1854	4507.28671
$f_{1113}^{(1)}$	−46694	−58337.72	−46694	−1841.45757
ρ_e /°	46.233	46.233	46.233	46.233
r_1^e /Å	1.18724	1.18724	1.18724	1.18724
a_1 /Å^{-1}	3.1848	3.1848	3.1848	3.1848

Table 3.1: Values of NO_2 potential parameters (in cm^{-1}) for potentials by: Tashkun and Jensen; Xie and Yan; Vilanove and Jacon; this work (see Chapter 4).

Level 0,0,0				Level 0,1,0				Level 1,0,0				Level 0,2,0			
	Obs	o-c	XY		Obs	o-c	XY		Obs	o-c	XY		Obs	o-c	XY
0_{00}	0.0	0.0	0.0	0_{00}	749.65	-0.24	-0.04	0_{00}	1319.79	-1.84	-0.29	0_{00}	1498.34	-1.84	-0.11
2_{02}	2.53	-0.03	-0.03	2_{02}	2.53	-0.03	-0.03	2_{02}	2.52	-0.02	-0.03	2_{02}	2.53	-0.02	-0.03
2_{20}	32.81	-0.42	-0.109	2_{20}	34.29	0.04	0.09	2_{20}	33.17	-0.52	0.04	2_{20}	35.89	-0.52	0.21
3_{22}	35.34	-0.45	-0.139	3_{22}	36.81	0.01	0.06	3_{22}	35.69	-0.55	0.01	3_{22}	38.42	-0.55	-0.19
4_{04}	8.44	-0.09	-0.098	4_{04}	8.43	-0.10	-0.09	4_{04}	8.39	-0.08	-0.09	4_{04}	8.42	-0.08	-0.01
4_{22}	38.72	-0.49	-0.178	4_{22}	40.19	-0.03	0.02	4_{22}	39.05	-0.58	-0.02	4_{22}	41.79	-0.58	0.15
4_{40}	129.06	-1.67	-0.447	4_{40}	134.82	0.15	0.31	4_{40}	130.47	-2.06	0.06	5_{24}	46.00	-0.62	0.10
5_{24}	42.94	-0.54	-0.229	5_{24}	44.41	-0.09	-0.03	5_{24}	43.24	-0.62	-0.07				
5_{42}	133.23	-1.76	-0.496	5_{42}	139.04	0.09	0.26	5_{42}	134.67	-2.10	0.02				

Table 3.2: Obs-calc's for a selection of rotational energy levels (in cm^{-1}) for work presented here ("o-c") and for XY potential (XY).

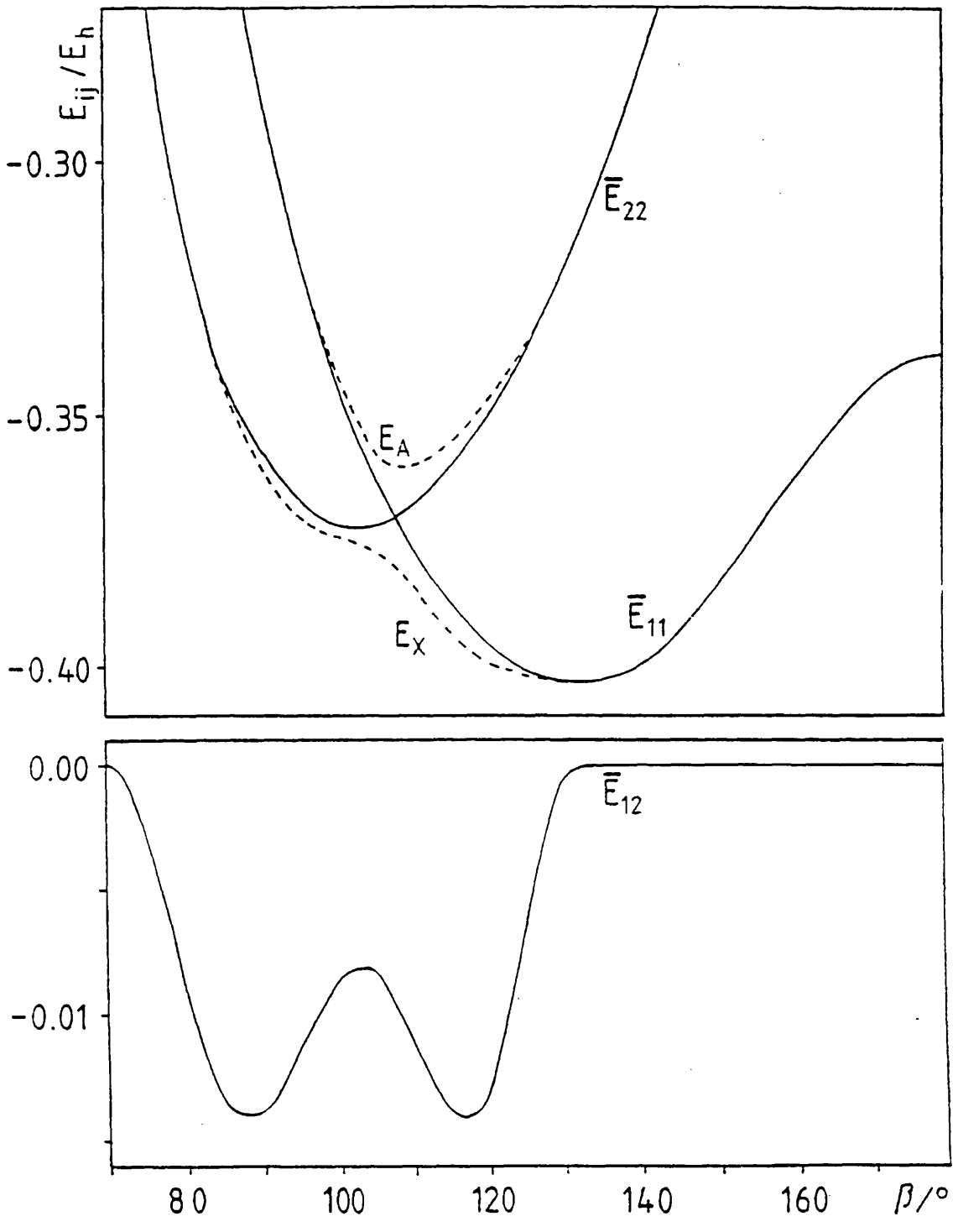

Figure 3.1: Calculated potential energy curves [62] for the lowest two electronic states of the NO_2 molecule in both the diabatic (solid curves) and adiabatic (dashed curves) representations with fixed values of $r_1 = r_e(\tilde{X}) = 2.2739400459\ a_0$ and $r_2 = 2.47\ a_0$. Note that the scale for the lower part of the figure is five times greater than that in the upper part.

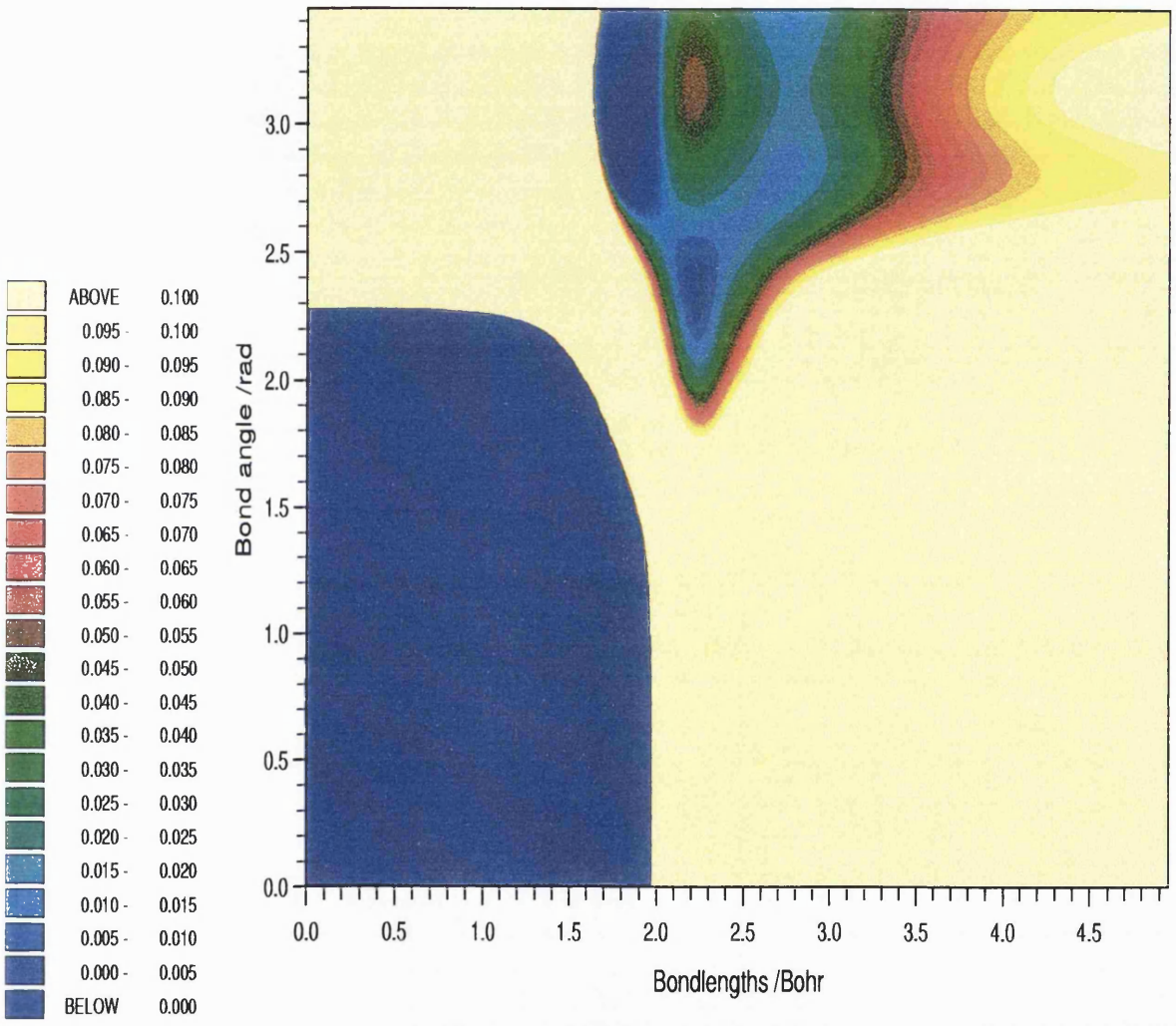

Figure 3.2: Contour plot of TJ NO_2 potential; symmetric stretch. The bondlengths are set to be equal. The energy scale is in Hartrees.

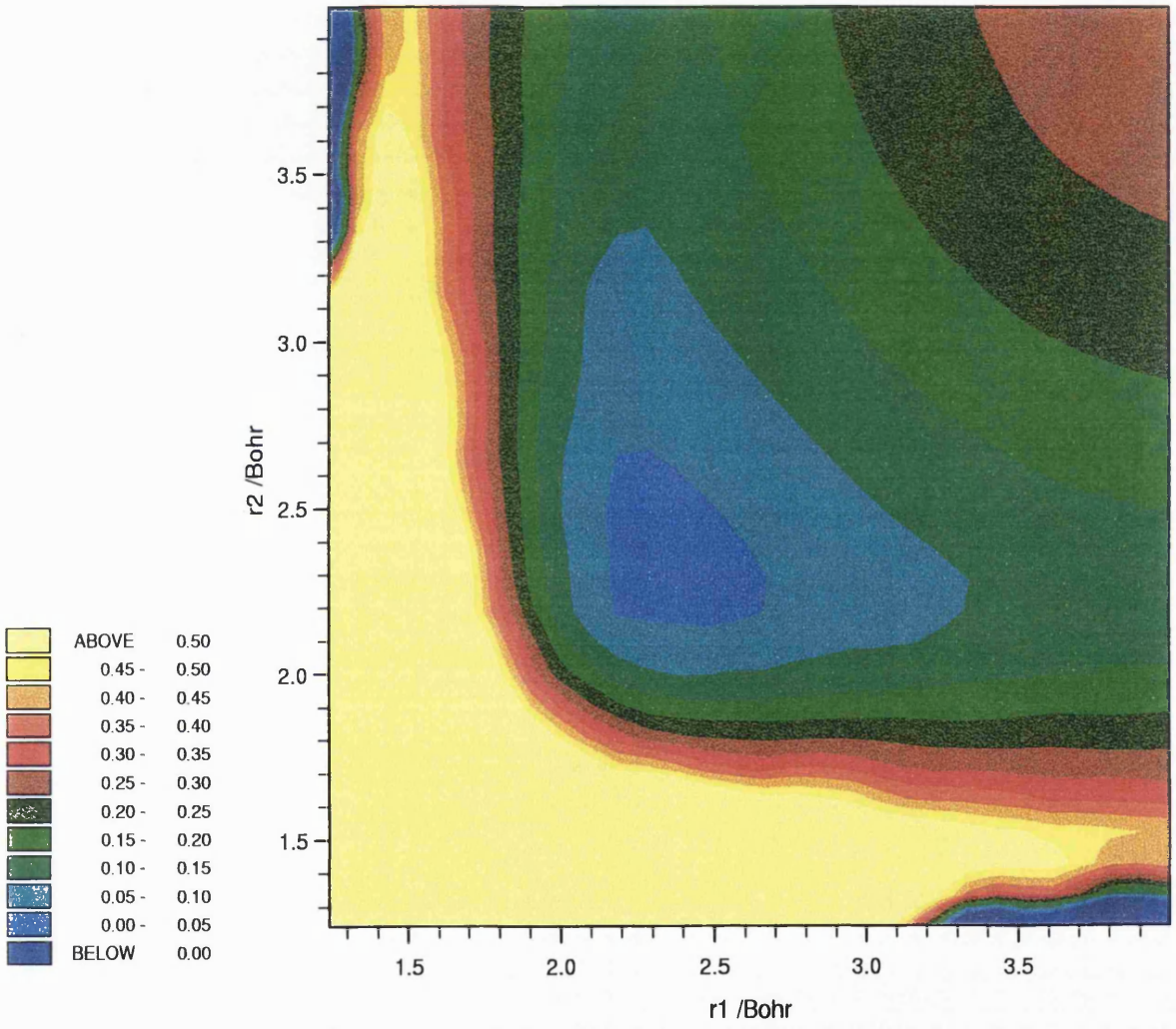

Figure 3.3: Contour plot of XY NO_2 potential; asymmetric stretch. The bond angle is frozen at equilibrium.

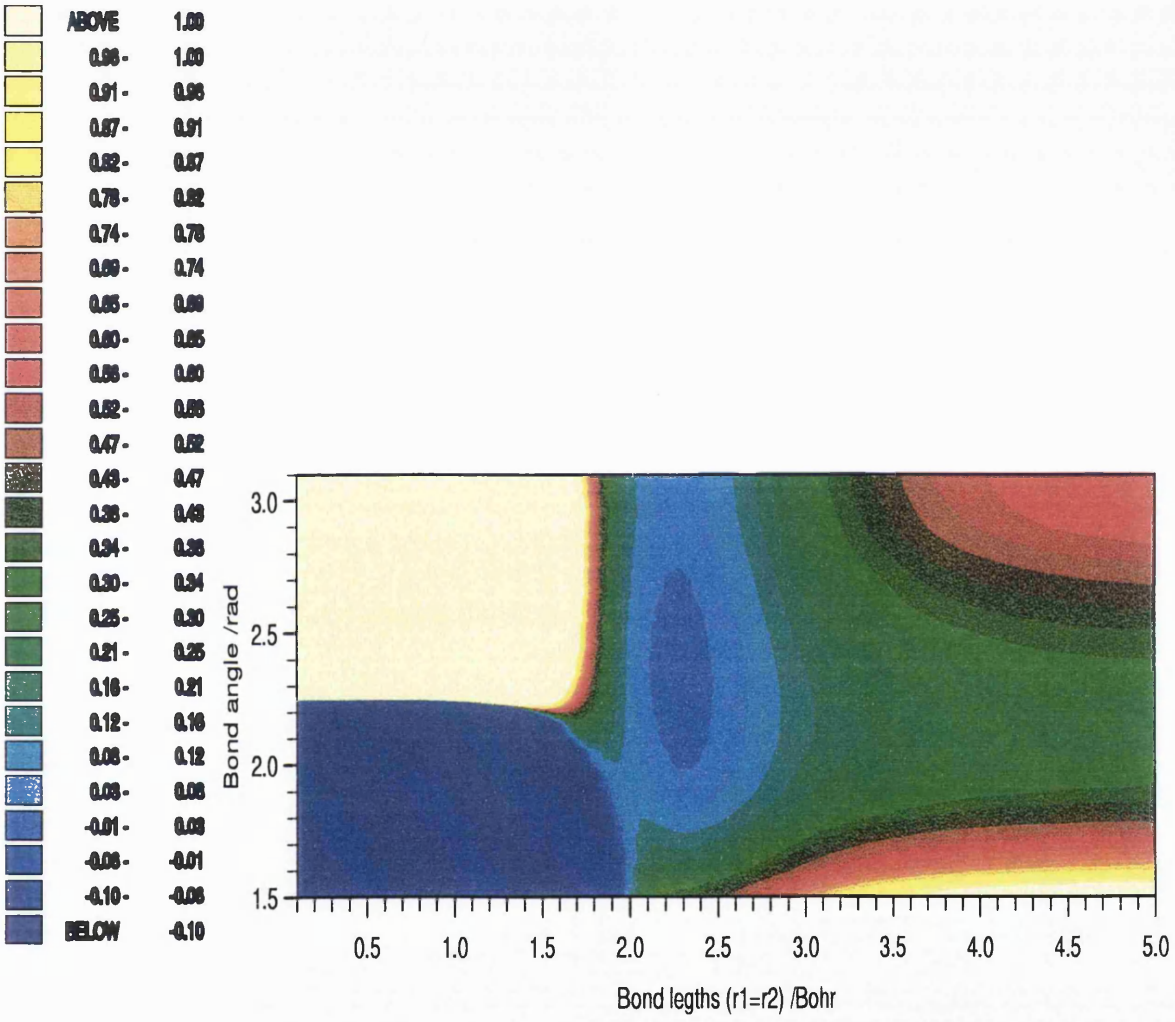

Figure 3.4: Contour plot of XY NO_2 potential; symmetric stretch.

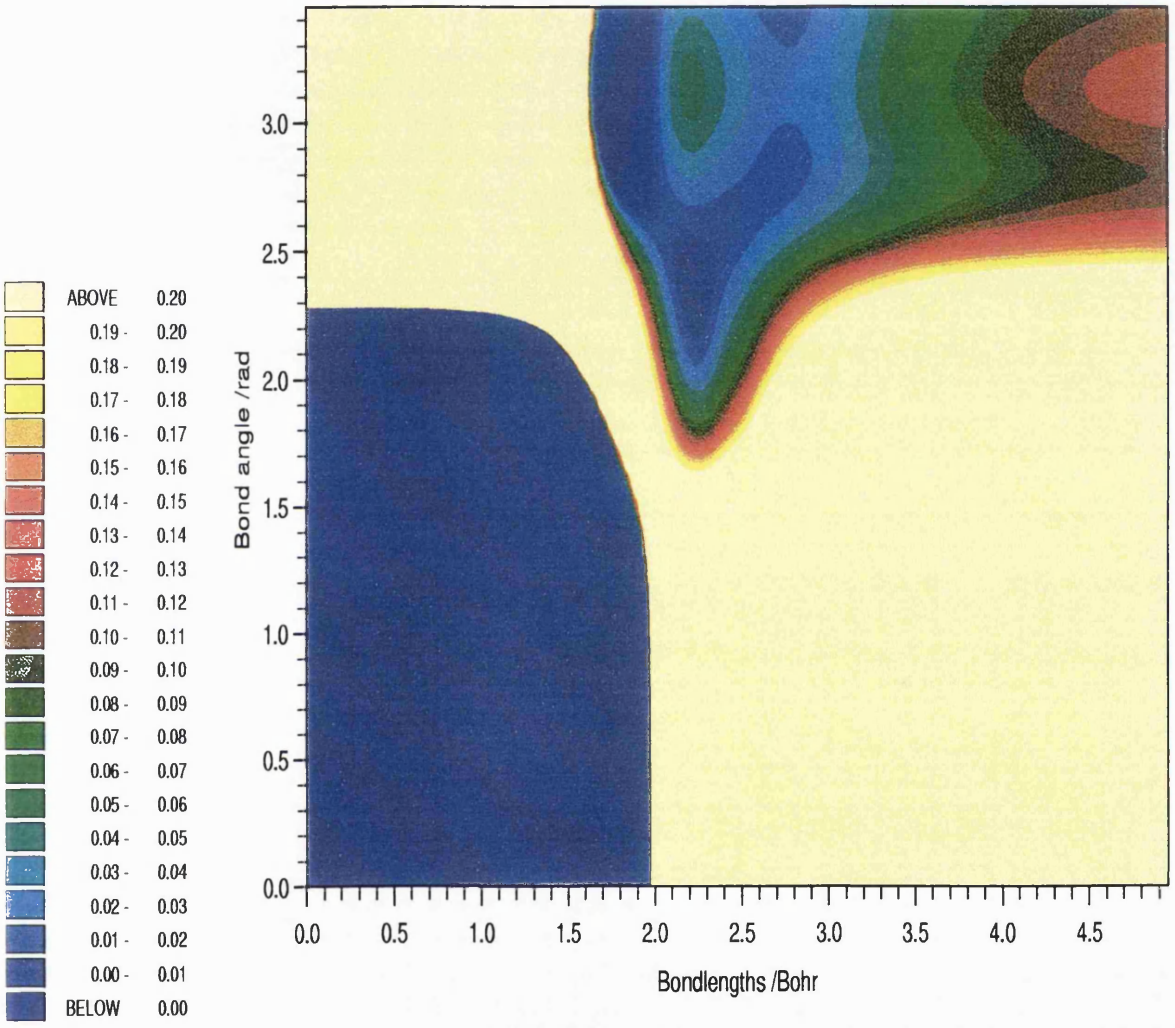

Figure 3.5: Contour plot of VJ NO_2 potential; symmetric stretch. The bondlengths are set to be equal.

Chapter 4

A New Fitted Potential for the Electronic Ground State of NO_2

4.1 The Potential Energy Function

For the potential energy function used in this work see 3.4.

4.2 Experimental Data

The vibrational term values used here were obtained by Delon and Jost [58] using Laser Induced Dispersed Fluorescence Spectroscopy (LIDFS) of jet cooled NO_2. They recorded the complete set of 191 vibrational levels below 10,000 cm^{-1} and some levels up to 12,000 cm^{-1}. The first electronically excited state lies at about 9,734 cm^{-1} above the vibrational ground state [58, 67].

The LIDFS of jet cooled NO_2 in emission from 11 different vibronic levels located between 22,006 and 23,625 cm^{-1} was recorded. These levels were 10 B_2 vibronic levels

and the $\tilde{B}^2B_1$ (0,8,0) level. For each band the $K = 0, N = 1, J = 3/2$ upper rotational level was selected as it was the brightest in the excitation spectrum. Also, it could be resolved rotationally and for fine structure (spin-splitting). The corresponding variety of Franck-Condon accesses allowed the observation of the complete set of 191 lowest vibrational levels of the $\tilde{X}^2A_1$ ground state located up to 10,000 cm^{-1}. The vibrational band origins were measured to within typically 0.3 cm^{-1}, assigned (n_1, n_2, n_3) and fitted with a 24 coefficient Dunham expansion giving a typical residual error of 0.5 cm^{-1}. Furthermore, the vibrationless $\tilde{A}^2B_2$ level was probably also observed at 9737 cm^{-1}. A perturbative model of the $\tilde{X}^2A_1$-$\tilde{A}^2B_2$ vibronic interaction was used in order to calculate the energy shift of the high vibrational levels (around 10,000 cm^{-1}) of the $\tilde{X}^2A_1$ state.

Data on the rotationally excited states is available for a number of low-lying vibrational states [75, 76]. However our calculations do not consider spin interaction effects and so we have used the deperturbed rotational data (see below) calculated by Kozin [70] for TJ. This data consists of rotational term values with $N \leq 5$ for the (0,0,0), (0,1,0), (1,0,0), (0,2,0) and (0,0,1) vibrational states.

The total angular momentum, $\underline{J}$, of a state is given by

$$\underline{J} = \underline{N} + \underline{S}, \tag{4.1}$$

where $\underline{N}$ is the rotational angular momentum and $\underline{S}$ is the spin angular momentum. In this case, $\underline{S} = 1/2$. So, deperturbed levels are levels quoted with e.g. $\underline{N} = 2$ rather than $\underline{J} = 5/2, 3/2$.

4.3 Calculations

Calculations of the vibrational terms were performed using the exact kinetic energy (EKE) DVR3D program [38]. For these calculations we used Radau coordinates, symmetrised radial grids based on Gauss-Laguerre quadrature with 37 DVR points and an angular grid using Gauss-Legendre quadrature with 115 DVR points. The dimension of the final Hamiltonian used to calculate the band origins was 1800.

Rotational calculations were performed using the ROTLEV3B program which is part of the DVR3D suite. ROTLEV3B performs the second step of a two-step variational calculation for the rovibrational states of triatomic molecules using an axis embedding which bisects the radau angle [6, 77]. Tests on both the vibrational and rotational steps of the calculation suggested that the basis sets used were actually somewhat larger than was required to obtain adequate convergence of the energy levels.

The derivatives of the potential constants with respect to changes in the energy levels were calculated using the Hellman-Feynman theorem. A new module, XPECT3, was written to perform this task within a DVR framework. See Subsection 4.3.1.

We attempted to use the original surface of TJ for EKE calculations of the band origins of NO_2. These calculations failed due to the presence of holes in certain areas of the potential. Analysis of TJ's potential suggested that these holes were caused by the large negative values of the parameters $f_{13}^{(3)}$ and $f_{1113}^{(1)}$ (see table 3.1).

Therefore, these parameters were reset to zero and a new fit, using the MORBID program, was attempted. There is a discrepancy between energy levels calculated using MORBID and those using an EKE operator due the approximation in the kinetic energy employed by MORBID. It has been noted previously [78] that the discrepancy is essentially constant with respect to changes in the potential parameters. Thus it was

possible to use the corrected MORBID levels for fitting once the correction factor had been determined. Using this technique a potential was constructed which had a similar standard deviation to TJ's but no spurious minima in physically important regions. This new potential was used as the starting point for fits using the EKE operator.

A least-squares fitting procedure was then implemented to find the optimum values for the potential parameters. These fits used a mixture of the sophisticated Interactive Non-Linear Least Squares (I-NoLLS) [79] program suite and a simpler Gauss-Newton minimization procedure.

4.3.1 The Hellmann-Feynman Theorem

The Hellmann-Feynman theorem states:

$$\frac{\partial E_n}{\partial p} = \left\langle \Psi_n \left| \frac{\partial H}{\partial p} \right| \Psi_n \right\rangle, \tag{4.2}$$

where $\partial H/\partial p$ is the derivative of the Hamiltonian with respect to a potential parameter, p, and Ψ_n are the wavefunctions of the energy levels. In fact this is only true where Ψ_n are the exact wavefunctions. It was therefore necessary initially to test the derivatives calculated using the Hellman-Feynman theorem by comparing them with numerically calculated derivatives. I.e. comparison with derivatives calculated by changing one parameter at a time by a small amount. The comparison showed that the derivatives calculated with the Hellman-Feynman theorem were highly accurate.

In this case,

$$H = K + V. \tag{4.3}$$

As K will not change with respect to the potential parameters, this means that equation 4.2 becomes:

$$\frac{\partial E_n}{\partial p} = \left\langle \Psi_n \left| \frac{\partial V}{\partial p} \right| \Psi_n \right\rangle, \tag{4.4}$$

The potential, V, can be described as,

$$V = \sum_{ijk} c_{ijk} F_{ijk}(q_1, q_2, q_3) \tag{4.5}$$

where c_{ijk} are the potential parameters. So, equation 4.4 can be written,

$$\frac{\partial E_n}{\partial p} = \langle \Psi_n | F_{ijk} | \Psi_n \rangle . \tag{4.6}$$

Since in a DVR scheme the wavefunction is simply given as an amplitude at each (α, β, γ) grid point,

$$\Psi_n(\alpha, \beta, \gamma) = d^n_{\alpha,\beta,\gamma}, \tag{4.7}$$

equation 4.6 can be written as a simple sum over all grid points:

$$\frac{\partial E_n}{\partial p} = \sum_{\alpha,\beta,\gamma} d^{n^2}_{\alpha,\beta,\gamma} F_{ijk}(\alpha, \beta, \gamma). \tag{4.8}$$

XPECT3 evaluates this expression using quadrature at the DVR points. This method of calculating derivatives is thus very rapid. It means that derivatives can be calculated for all potential parameters even if ultimately many of these will be frozen in the fit.

4.3.2 Least-Squares Fitting

A least-squares fitting procedure was implemented to find the optimum values for the potential parameters.

Least-squares fitting can be defined as the minimisation of

$$\chi^2 = \sum_{i=1}^{n} \left[\frac{y_i^{obs} - y_i^{calc}(p_1 \ldots p_m)}{\sigma_i} \right]^2 \tag{4.9}$$

where y^{obs} are observed values, y^{calc} are the corresponding calculated values, σ_i are the uncertainties associated with the data points and $p_1 \ldots p_m$ are the adjustable parameters.

To begin considering how to improve a trial p, first express y^{calc} as a Taylor series expansion about the current p

$$y^{calc}(p + x) = y^{calc}(p) + Jx + \ldots \tag{4.10}$$

where x is a small change in p. The $n \times m$ matrix J is the 'Jacobian' matrix of first partial derivatives of the calculated properties with respect the model parameters:

$$J_{ij} = \frac{\partial y_i^{calc}}{\partial p_j}. \tag{4.11}$$

Define the vector of differences thus,

$$d = y^{obs} - y^{calc}(p) = y^{obs} - y(p). \tag{4.12}$$

For a weighted least-squares fit a diagonal matrix G with non-zero elements is defined

$$G_{ii} = \frac{1}{\sigma_i}. \tag{4.13}$$

If we assume that the model function $y(p)$ is locally linear in p then we may neglect all but the first two terms in the expansion 4.10 and re-express problem 4.9 as: minimise,

$$||Ax - b||_2^2 \tag{4.14}$$

where $A = GJ$ and $b = Gd$ and the notation $||.||_2$ denotes the Euclidean length of a vector. Therefore the objective is to find an optimum vector x describing a step through parameter space. x is the parameter step corresponding to the well-known Gauss-Newton algorithm [80].

The method of performing a least-squares fit for this potential is, in itself, not unusual. However, each iteration is very expensive in computer time. It is therefore very important to minimise the number of iterations used.

We used more than one fitting routine to try to optimise our potential. One of the programs used was I-NoLLS [79]. This stands for Interactive Non-Linear Least Squares. The interactive nature of the program allows the user to exercise greater control over the fit than is usually possible. I-NoLLS allows the exclusion of any data points or parameters from the fit producing trial values for the subsequent iteration. The user can then conveniently choose which is the best way to proceed. Another advantage of I-NoLLS is that it is designed to cope with non-linear problems. Using a standard Gauss-Newton least squares algorithm [80] the step in parameter space would be correct only for a linear problem. Physical problems such as the fitting of a PES are certainly not linear. One solution to this problem is just to scale down the Gauss-Newton step by some factor in order to avoid taking too large a step in parameter space and thus overshooting, possibly greatly, the correct values. A superior method for non-linear problems is used by I-NoLLS. It uses Singular Value Analysis [81] which essentially breaks down the

Gauss-Newton step into several components in parameter space some of which are better defined than others. The I-NoLLS user can thus choose to take a parameter step along only the better defined "singular directions". This would not actually minimise the sum of squares of errors for a linear problem but for a non-linear problem it often provides a large reduction for a small step in parameter space. This reduces the chance of taking a non-physical parameter step (possible due to non-linearity) or of reaching a non-physical part of parameter space. I-NoLLS also has other features and uses further techniques to fits of non-linear problems as described in [79]. Since I-NoLLs only became available while the work presented here was being executed, a simpler Gauss-Newton based fitting routine was mainly used.

4.3.3 Convergence

Convergence tests were performed on the calculation of the band origins and on the rotational calculations. In table 4.1, the column "Original value" lists the values for various input parameters used to calculate the energy levels. The table shows values for a number of DVR3D [38] parameters that were altered to test convergence. NPNT2 is the number of DVR points in $r2$ from Gauss-(associated) Laguerre quadrature. NALF is the number of DVR points in θ from Gauss-(associated) Laguerre quadrature. MAX3D is the maximum size of the final Hamiltonian. r_e and D_e are morse parameters for the $r1$ coordinate. NVIB is the number of vibrational levels from DVR3D used by ROTLEV3B for each k to be read in the second variational step. IBASS is the number of vibrational levels selected by an energy ordering criterion in ROTLEVB. The assignments for the vibrational levels, in energy order, are (0,1,0), (0,0,4) and (2,4,2). As can be seen from the table, the results from using these parameters were, if anything, over-converged.

Even approaching 10,000 cm^{-1} it is clear that there are no convergence problems.

4.4 Removal of poorly fitted levels

We initially tried to determine the potential using all 114 even levels and 77 odd levels below 10,000 cm^{-1}. Fitting of the NO_2 surface is complicated by the intersection between the ground electronic state and the first excited state which is at approximately 10,000 cm^{-1}. The interaction between these two states perturbs the energy levels of the ground state. During the fitting procedure we removed several levels from the fit as they appeared not to be improving. It was assumed that this was because of the interactions with the higher state.

Most of the states removed, which are labelled in tables 4.3 and 4.4, have the common feature that they have a large value for v_2. It is also notable that in the region covered by XY's calculations, the levels we removed are those which are systematically too low in their calculation. Above about 9,500 cm^{-1}, many even levels were removed. It is clear from LPHB's calculation (see fig. III of ref [67]) that nearly all states in this region are strongly perturbed by vibronic interactions. Conversely we found it unnecessary to remove any odd states below the (4,0,3) level at 9531 cm^{-1}. The work of LPHB shows that the lower odd states are much less sensitive to vibronic effects than the corresponding even states, and that the (4,0,3) state is indeed the first one to be strongly perturbed.

4.5 Adding of additional potential parameters

The constants that were initially fitted were: $f_0^{(2)}$, $f_0^{(3)}$, $f_0^{(4)}$, $f_1^{(1)}$, $f_1^{(2)}$, $f_{11}^{(0)}$, $f_{11}^{(1)}$, $f_{13}^{(0)}$, $f_{111}^{(1)}$ $f_{113}^{(1)}$, $f_{1113}^{(0)}$. We reached the limit of the improvements that could be made by fitting

Parameter	Original value	Parameter Change	Level cm^{-1}	Change in Level cm^{-1}
NPNT2	37	+2	750.17209674	−0.00000001
			6279.18426584	+0.00000001
			8551.37079266	−0.00002090
NALF	115	+20	750.17209674	−0.00000005
			6279.18426584	+0.00000051
			8551.37079266	+0.00002721
MAX3D	1800	+200	750.17209674	−0.00000014
			6279.18426584	−0.00000018
			8551.37079266	−0.00000281
r_e	2.81	−0.01	750.17209674	−0.00000003
			6279.18426584	−0.00000002
			8551.37079266	+0.00002620
		−0.04	750.17209674	−0.00000004
			6279.18426584	−0.00000004
			8551.37079266	+0.00033012
D_e	1.3	+0.1	750.17209674	−0.00000003
			6279.18426584	−0.00000007
			8551.37079266	−0.00000095
IBASS/NVIB	750/150	+750/+50	4.267174731	−0.000000000
			34.94004943	−0.000000000
			754.1591906	−0.0000000
			6911.244466	−0.000018

Table 4.1: Convergence tests. This table shows values for a number of DVR3D [38] parameters that were altered to test convergence. See section 4.3.3 for an explanation on the parameters.

these parameters. However, these constants were well determined and the correlation between them was very low, we therefore investigated whether the potential could be improved by allowing more higher order constants in the potential to float during the fit.

We were able to determine the additional constants $f_1^{(3)}$, $f_{11}^{(2)}$, $f_{13}^{(1)}$, $f_{13}^{(2)}$, $f_{113}^{(0)}$ and $f_{1113}^{(1)}$. Of these seventeen potential parameters, $f_{111}^{(1)}$ was found to be very poorly determined so it was discarded from the list of parameters that we tried to fit. We also tried to fit $f_0^{(5)}$, $f_{111}^{(0)}$ and $f_{1111}^{(0)}$ but found that we could not determine meaningful values for them.

Final values for the optimized potential constants are given in table 4.2. The errors given in this table are the statistical errors found in the last iteration of the fit. They therefore give some idea as to how well individual constants have been determined by the fit. Of course these errors make no allowance for any systematic errors in the procedure that we employed.

4.6 Levels above 10,000 cm^{-1}

After fitting the potential as well as possible to the data available up to 10,000 cm^{-1}, we tried to fit it to the available data up to 12,000 cm^{-1}. Scatter plots in figures 4.1 and 4.2 show the values of the obs-calcs for our best potential for the ranges 0-10,000 cm^{-1} and 0-12,000 cm^{-1} respectively. The second plot clearly shows the difficulty of reproducing the levels above 10,000 cm^{-1}. Even when we removed the levels with the worst agreement we were unable to make any significant reduction in the standard deviation. We believe that this problem stems from the interaction of the ground state with higher electronic states and non-Born-Oppenheimer effects.. However, despite these problems associated with NO_2, figure 4.2 demonstrates that it is possible to do meaningful calculations for this molecule using a single surface. See Section 4.8 for further comments.

4.7 The Final Potential

The final version of the potential is illustrated in figures 4.3 and 4.4. Figure 4.3 is a contour plot of the symmetric stretch. Figure 4.4 is a similar plot in the asymmetric stretch. As can be seen in this figure there are holes in our potential but they are not close to any meaningful areas and have not prevented any computations on the surface.

4.8 Comparison With Experimental Data

Before the final fitting procedure the standard deviation of the levels included in the fit at that time was 8.0 cm^{-1}. The final standard deviation achieved after fitting, and after the levels listed were removed, was 2.8 cm^{-1}.

As mentioned above, the experimental data we used for fitting and comparison purposes was that of Delon and Jost [58]. For a comparison of our calculated vibrational term values with those of Delon and Jost see tables 4.3 and 4.4. As can be seen from the asterisked levels, most of those that were removed from the fit remained poorly fitted. The values for levels (4,2,2) and (0,9,2) improved considerably. It is not particularly surprising that some of the removed levels became much better determined. The criterion for the removal of a level was that it was poorly determined. Levels were not removed because of any other characteristic.

The reason for the poor reproduction of some of the higher lying levels is unclear. It is difficult to be certain whether the large obs-calc values are due only to deficiencies of the potential or if they are due to the pertubing effect of interactions with excited levels.

Tables 4.5 and 4.6 quote the observed-calculated values for levels above 10,000 cm^{-1} for which we were able to make reasonable assignments. It is clear that calculations with

the new potential above 10,000 cm^{-1} are much less good than those at lower energy.

It is equally clear that below 10,000 cm^{-1} a good fit has been achieved with experimental observations (see tables 4.3 and 4.4.) This has been accomplished using only one effective potential energy surface. Due to the way that the surface was constructed (i.e. by fitting to observed results), it "contains" (i.e. takes into account) non-Born-Oppenheimer effects.

We used our optimized potential to calculate rovibrational levels up to $N = 5$. We used the vibrational and rotational term values quoted by Tashkun and Jensen [68] for purposes of comparison. The agreement of these levels with experiment was good. The error in observed minus calculated energies was found to vary from 0.008 cm^{-1} to around 2 cm^{-1}, see table 4.7.

4.9 Conclusions and Further Work

Tests on previous spectroscopically determined potentials have shown that some of these have problems. In particular a seemingly excellent water potential was found to give unacceptably poor results for rotationally excited states, while several ground state NO_2 potentials were found to contain unphysical minima ('holes').

We have significantly improved the spectroscopically determined potential for the electronic ground state of NO_2 constructed potential for the electronic ground state of NO_2 constructed by Tashkun and Jensen [68]. This improvement has been achieved by use of a Hamiltonian based on the use of an exact kinetic energy operator and by taking care to eliminate artificial holes from physical regions of the potential.

Unlike most previous spectroscopic determinations of NO_2 potentials [67, 71, 74] and Xie and Yan's recent water potential [72], we have tested our new potential against

rotational term values for NO_2. We regard this step as vital for proving that the potential obtained is indeed physical.

Finally one must remember that NO_2 is actually a classic case of Born-Oppenheimer failure. In this work we have performed our fits to a single potential function, representing the electronic ground state of the system. However non-adiabatic calculations on this system by Hirsch, Buenker and Petrongolo [64, 67] strongly suggest that many vibrational states lying 5,000 cm^{-1} or more above the vibrational ground state are perturbed by interactions with the low-lying $\tilde{A}\ ^2B_2$ state. As the majority of the vibrational levels used in this work lie in this perturbed region, the resulting potential energy surface must be regarded as an effective one which in some part includes contributions from these non-adiabatic interactions.

Future work on NO_2 would be to consider such non-Born-Oppenheimer effects. This would require a surface for each of the lowest three electronic states of NO_2. Off-diagonal, non-Born-Oppenheimer coupling elements (eg from Petrolongo *et al* [63, 62, 64, 66, 67] would also be require to construct the Hamiltonian matrix. The ultimate aim would be to determine true surfaces (rather than an effective ground state surface) for the ground and excited electronic states.

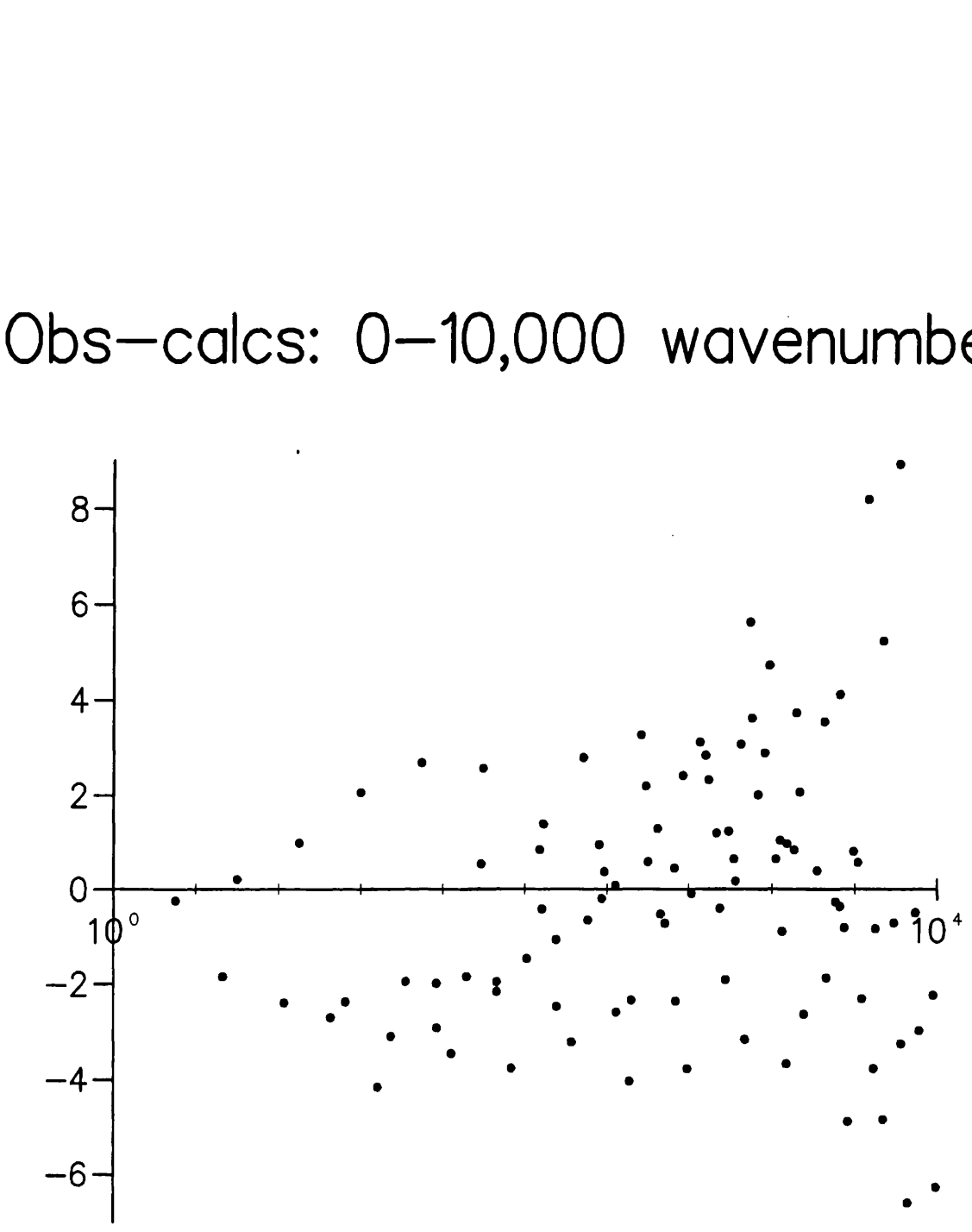

Figure 4.1: Scatter plot of obs-calcs for the new NO_2 potential. Levels up to 10,000 cm^{-1} are plotted on the x-axis against obs-calc in cm^{-1}.

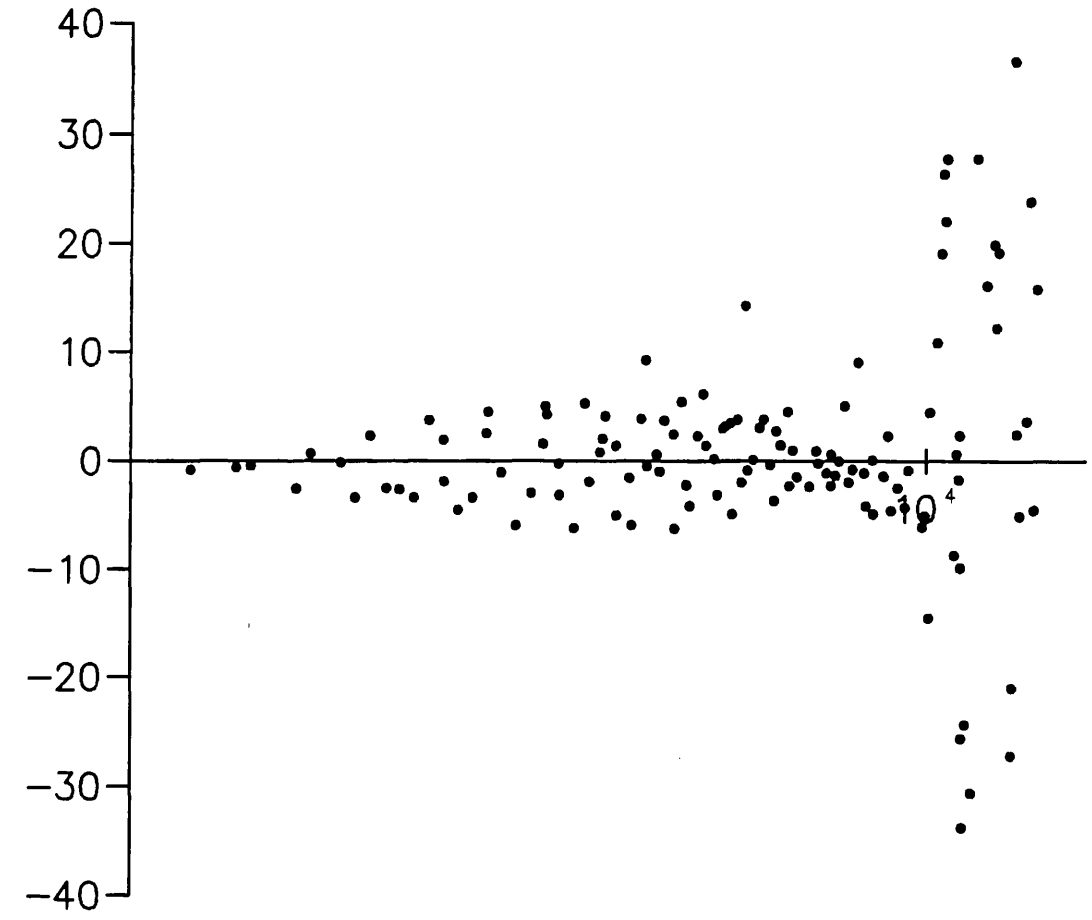

Figure 4.2: Scatter plot of obs-calcs for the new NO_2 potential. Levels up to 12,000 cm^{-1} are plotted on the x-axis against obs-calc in cm^{-1}.

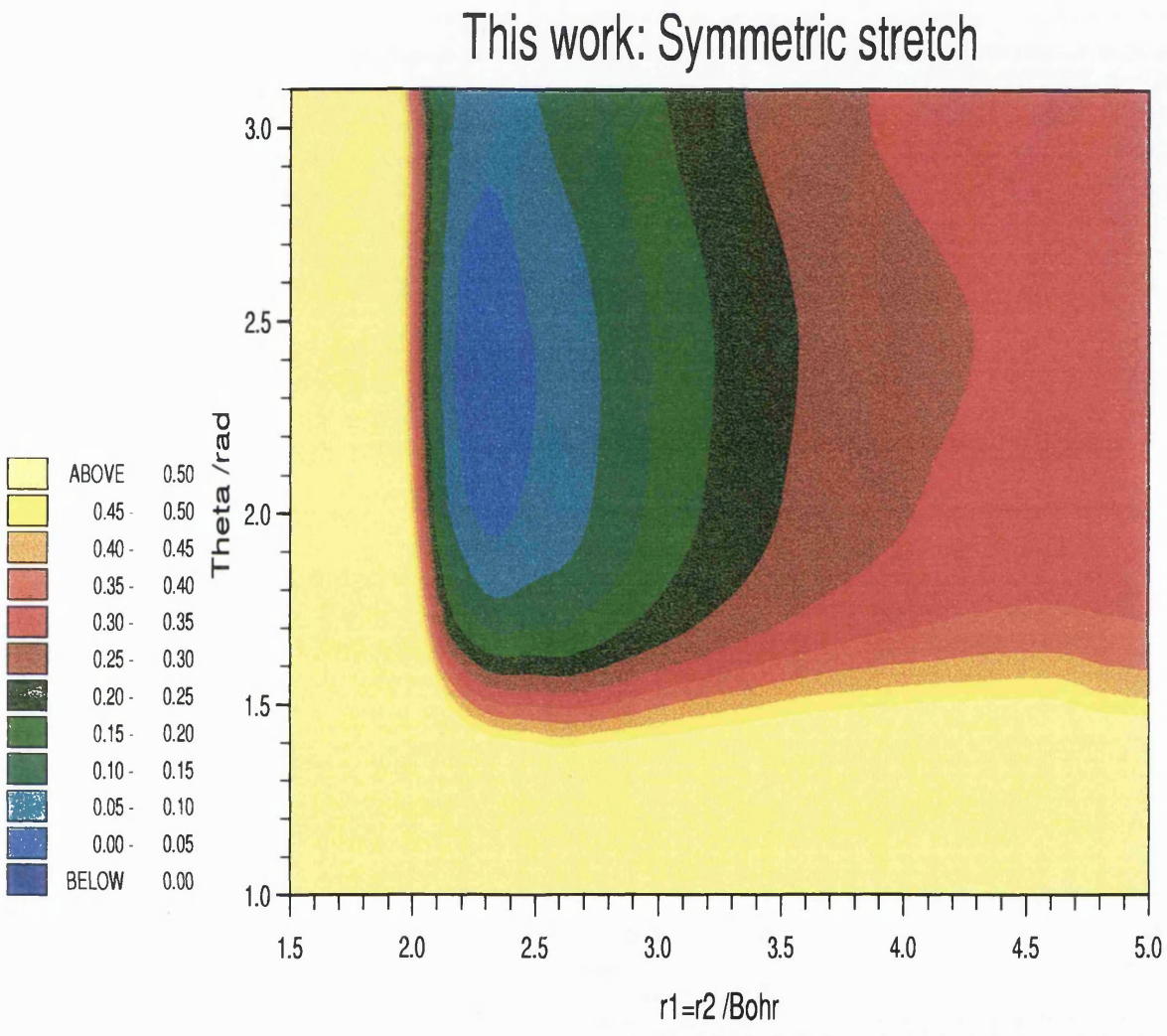

Figure 4.3: Symmetric stretch for new NO_2 potential. r1 and r2 have been frozen equal and plotted against the bond angle.

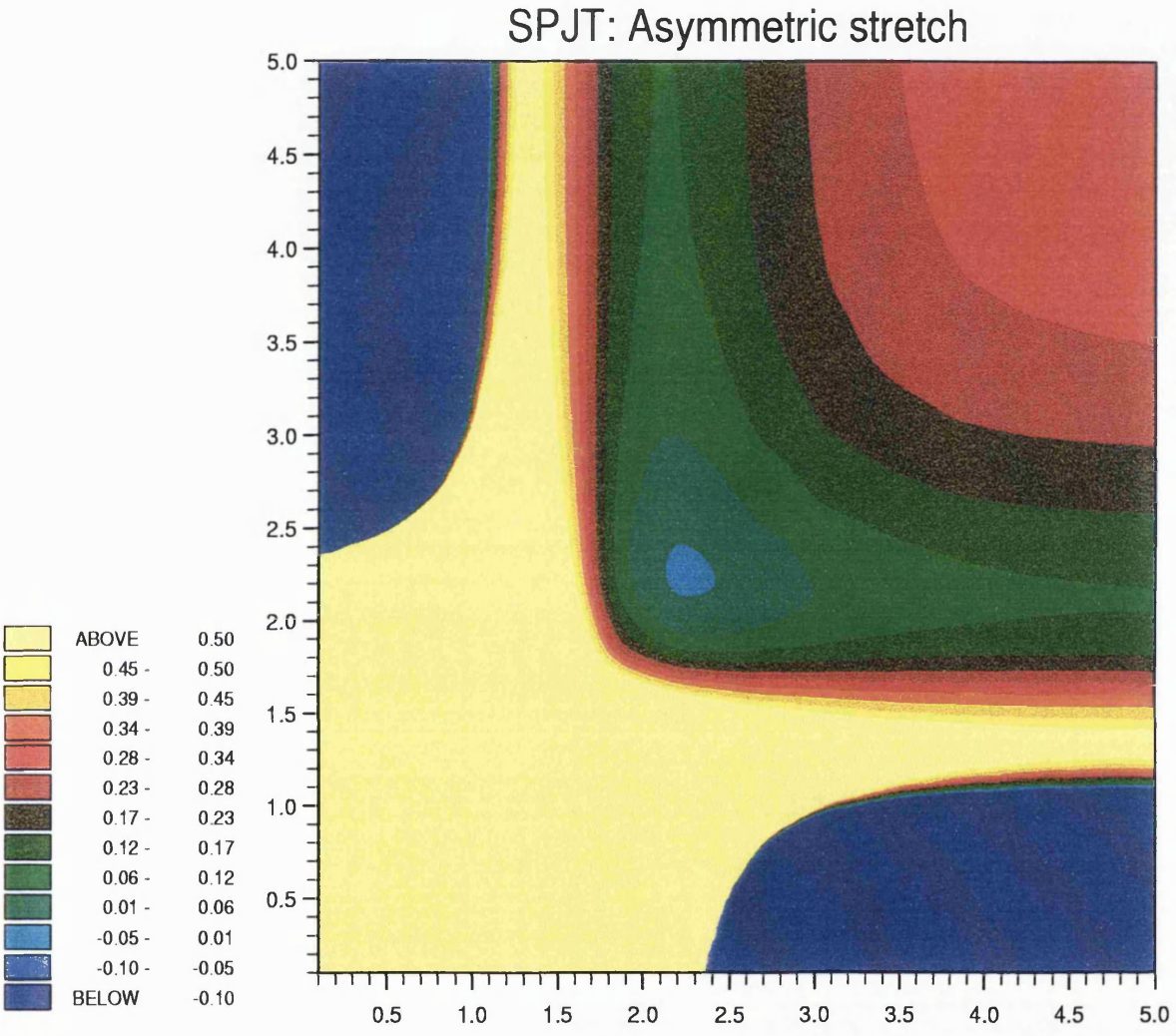

Figure 4.4: Asymmetric stretch for new NO_2 potential showing r_1 against r_2 (in Bohr) with the bond angle fixed at equilibrium. Holes can be seen but they are not in a significant region of the potential.

Parameter	Value /cm^{-1}	Error /cm^{-1}
$f_0^{(2)}$	78259.20740	51
$f_0^{(3)}$	−107129.99582	358
$f_0^{(4)}$	225437.38541	307
$f_1^{(1)}$	−9514.44438	107
$f_1^{(2)}$	−33493.10799	467
$f_1^{(3)}$	−3080.26035	325
$f_{11}^{(0)}$	27019.00973	14
$f_{11}^{(1)}$	16052.75505	271
$f_{11}^{(2)}$	652.42584	236
$f_{13}^{(0)}$	9106.89156	40
$f_{13}^{(1)}$	1094.98984	570
$f_{13}^{(2)}$	7446.65832	802
$f_{113}^{(0)}$	−410.29378	142
$f_{113}^{(1)}$	−1567.88852	514
$f_{1113}^{(0)}$	4507.28671	26
$f_{1113}^{(1)}$	−1841.45757	159
ρ_e /°	46.233	
r_1^e / Å	1.18724	
a_1 /Å^{-1}	3.1848	

Table 4.2: Non-zero NO_2 potential parameters determined in our final least squares fit.

(ν_1,ν_2,ν_3)	Obs	O−C	(ν_1,ν_2,ν_3)	Obs	O−C	(ν_1,ν_2,ν_3)	Obs	O−C
0,1,0	749.64	−0.24	5,0,0	6475.05	2.18	5,3,0	8623.34	3.55
1,0,0	1319.79	−1.85	1,7,0	6497.60	0.58	2,0,4	8652.27	−1.87
0,2,0	1498.34	0.22	1,3,2	6616.53	1.29	1,10,0	8690.72	7.98*
1,1,0	2063.12	−2.39	4,2,0	6653.54	−0.53	1,6,2	8758.28	−0.26
0,3,0	2246.04	0.98	0,9,0	6705.23	−0.72	4,5,0	8809.81	4.12
2,0,0	2627.34	−2.70	0,5,2	6823.80	0.45	4,1,2	8817.61	−0.36
1,2,0	2805.60	−2.37	3,4,0	6837.75	−2.36	1,2,4	8868.35	−0.82
0,4,0	2993.00	2.05	3,0,2	6921.67	2.41	0,12,0	8911.29	−4.89
0,0,2	3201.44	−4.17	0,1,4	6979.21	−3.78	7,0,0	8968.55	8.78*
2,1,0	3364.57	−3.10	2,6,0	7029.48	−0.09	0,8,2	8982.08	0.81
1,3,0	3547.10	−1.95	2,2,2	7125.60	3.11	3,7,0	9003.53	9.70*
0,5,0	3738.60	2.68	5,1,0	7193.35	2.84	3,3,2	9031.81	0.57
3,0,0	3922.61	−1.98	1,8,0	7231.06	2.32	0,4,4	9082.71	−2.32
0,1,2	3929.12	−2.92	1,4,2	7332.45	1.19	6,2,0	9151.35	8.21
2,2,0	4100.58	−3.46	4,3,0	7374.57	−0.40	2,9,0	9203.99	15.59*
1,4,0	4286.82	−1.84	0,10,0	7443.09	−1.92	0,0,6	9226.23	−3.78
1,0,2	4461.07	0.53	1,0,4	7478.02	1.24	2,5,2	9247.78	−0.84
0,6,0	4482.57	2.55	0,6,2	7544.62	0.65	5,0,2	9295.48	−8.76*
3,1,0	4652.00	−2.16	3,5,0	7562.47	0.18	5,4,0	9334.06	5.25
0,2,2	4656.34	−1.95	3,1,2	7627.14	3.08	2,1,4	9341.17	−4.85
2,3,0	4835.05	−3.77	0,2,4	7681.49	−3.16	1,11,0	9416.05	12.66*
1,5,0	5025.20	−1.47	6,0,0	7730.08	5.63	1,7,2	9468.38	−0.71
1,1,2	5180.54	0.84	2,7,0	7757.29	3.63	4,2,2	9511.96	0.30*
4,0,0	5205.81	−0.42	2,3,2	7834.97	2.00	4,6,0	9524.14	8.94
0,7,0	5224.55	1.38	5,2,0	7909.46	2.89	1,3,4	9561.06	−3.26
0,3,2	5377.91	−1.07	1,9,0	7962.27	4.73	0,13,0	9640.29	−6.60
3,2,0	5384.41	−2.47	1,5,2	8046.44	0.64	7,1,0	9672.18	9.97*
2,4,0	5568.41	−3.22	4,4,0	8093.61	1.04	0,9,2	9696.16	1.83*
2,0,2	5701.41	2.79	4,0,2	8120.70	−0.90	3,8,0	9716.70	12.72*
1,6,0	5762.23	−0.65	1,1,4	8174.27	0.97	3,4,2	9731.72	−0.50
1,2,2	5898.94	0.95	0,11,0	8178.27	−3.68	0,5,4	9780.98	−2.99
4,1,0	5930.66	−0.19	0,7,2	8264.28	0.83	3,0,4	9796.80	−15.01*
0,8,0	5965.61	0.38	3,6,0	8284.17	3.74	6,3,0	9855.68	7.63*
0,4,2	6101.80	0.09	3,2,2	8330.35	2.06	0,1,6	9904.99	8.33*
3,3,0	6112.11	−2.59	0,3,4	8382.64	−2.64	2,10,0	9920.43	10.15*
0,0,4	6275.98	−4.04	6,1,0	8441.44	6.69*	2,6,2	9950.41	−2.24
2,5,0	6299.70	−2.34	2,8,0	8482.12	8.52*	5,1,2	9984.14	−6.28
2,1,2	6414.16	3.27	2,4,2	8542.25	0.40			

Table 4.3: Observed even symmetry vibrational term values [58] and observed minus calculated values /cm^{-1}. An asterisk indicates that a level was removed from the fit.

(ν_1,ν_2,ν_3)	Obs	O−C	(ν_1,ν_2,ν_3)	Obs	O−C	(ν_1,ν_2,ν_3)	Obs	O−C
0,0,1	1616.85	−2.78	3,2,1	6872.10	2.76	4,3,1	8797.95	3.21
0,1,1	2355.15	−2.44	0,3,3	6897.37	−1.35	1,4,3	8816.65	0.57
1,0,1	2906.07	−0.69	2,4,1	7072.23	0.92	1,0,5	8941.28	0.63
0,2,1	3092.48	−1.51	2,0,3	7192.23	1.89	0,10,1	8944.50	−1.65
1,1,1	3637.84	−0.56	1,6,1	7277.83	1.13	3,5,1	9008.77	1.48
0,3,1	3829.34	0.16	4,1,1	7386.33	4.74	0,6,3	9029.44	−0.70
2,0,1	4179.94	1.34	1,2,3	7403.04	1.97	3,1,3	9065.47	−1.05
1,2,1	4369.10	0.26	0,8,1	7492.23	1.69	6,0,1	9101.27	−2.80
0,4,1	4564.22	0.87	3,3,1	7587.04	2.43	0,2,5	9148.84	−3.17
0,0,3	4754.21	−4.59	0,4,3	7609.57	−0.46	2,7,1	9220.73	2.62
2,1,1	4905.52	1.86	0,0,5	7766.28	−3.86	2,3,3	9281.74	2.20
1,3,1	5098.00	−0.04	2,5,1	7791.18	1.24	5,2,1	9310.32	−0.81
0,5,1	5298.16	1.54	2,1,3	7888.16	3.76	1,9,1	9436.85	1.23
3,0,1	5437.54	3.11	5,0,1	7903.54	1.17	1,5,3	9500.17	2.42
0,1,3	5469.66	−3.69	1,7,1	8000.93	1.84	4,4,1	9518.26	−3.11
2,2,1	5630.36	2.64	4,2,1	8093.10	3.90	4,0,3	9531.08	−16.26*
1,4,1	5826.29	0.41	1,3,3	8110.13	1.09	1,1,5	9623.58	−1.66
1,0,3	5984.71	1.06	0,9,1	8218.84	−0.43	0,11,1	9654.17	−16.46*
0,6,1	6030.71	1.73	3,4,1	8299.45	1.96	3,6,1	9713.52	0.23
3,1,1	6156.25	3.87	0,5,3	8320.00	−0.55	0,7,3	9736.30	−2.30
0,2,3	6183.61	−2.94	3,0,3	8374.58	−3.83	3,2,3	9753.30	−2.49
2,3,1	6351.40	0.99	0,1,5	8457.15	−4.53	6,1,1	9797.03	−4.99
1,5,1	6552.84	0.66	2,6,1	8507.33	1.57	0,3,5	9836.38	−5.00
4,0,1	6676.86	4.29	2,2,3	8585.54	3.44	2,8,1	9928.47	2.35
1,1,3	6693.12	0.52	5,1,1	8608.92	1.31	2,4,3	9976.50	0.86
0,7,1	6761.44	1.09	1,8,1	8721.11	2.18			

Table 4.4: Observed odd symmetry vibrational term values [58] and observed minus calculated values /cm^{-1}. An asterisk indicates that a level was removed from the fit.

(ν_1,ν_2,ν_3)	Obs	O−C	(ν_1,ν_2,ν_3)	Obs	O−C	(ν_1,ν_2,ν_3)	Obs	O−C
2,2,4	10025.10	−11.96	6,0,2	10445.42	−36.71	0,15,0	11071.05	−21.08
5,5,0	10043.14	11.13	3,1,4	10478.49	−24.75	6,1,2	11096.84	37.94
1,12,0	10132.49	14.51	0,6,4	10486.21	−61.41	3,6,2	11126.61	2.73
8,0,0	10184.66	7.97	6,4,0	10557.69	−31.72	3,2,4	11170.56	−8.99
4,3,2	10203.86	27.08	0,2,6	10582.51	−94.01	0,7,4	11218.66	78.26
4,7,0	10231.98	25.27	2,11,0	10632.76	36.76	6,5,0	11259.79	69.76
1,4,4	10251.59	37.01	5,6,0	10746.29	19.80	0,3,6	11251.48	12.01
0,14,0	10352.09	−10.21	1,13,0	10850.34	26.42	5,3,2	11290.61	22.95
7,2,0	10375.23	−0.71	1,9,2	10876.58	6.03	2,8,2	11347.04	0.16
1,0,6	10399.71	5.61	4,4,2	10900.00	21.18	2,12,0	11364.34	63.90
0,10,2	10415.48	−1.61	1,5,4	10963.15	56.66	9,0,0	11376.13	13.16
3,5,2	10425.39	−5.05	1,1,6	11041.86	90.23	5,7,0	11440.88	69.18
3,9,0	10435.41	−29.62	7,3,0	11063.22	−15.90			

Table 4.5: Observed even symmetry vibrational term values [58] and observed minus calculated values /cm^{-1} for levels above 10,000 cm^{-1}. There are problems with assigning the levels correctly and it is unlikely that all the levels in the table are correctly assigned.

(ν_1,ν_2,ν_3)	Obs	O−C	(ν_1,ν_2,ν_3)	Obs	O−C	(ν_1,ν_2,ν_3)	Obs	O−C
5,3,1	10007.48	−4.87	0,12,1	10363.42	−28.40	2,5,3	10663.33	−33.23
2,0,5	10081.20	−9.27	0,8,3	10436.26	−9.60	5,4,1	10697.01	−13.33
1,10,1	10161.31	13.01	6,2,1	10488.24	−9.83	2,1,5	10763.15	−6.40
1,6,3	10200.29	2.56	0,4,5	10522.92	−7.07	1,11,1	10864.15	8.43
4,1,3	10214.37	−9.51	2,9,1	10630.89	2.28	4,6,1	10916.81	9.20
7,0,1	10270.88	43.94	5,0,3	10649.59	−10.88			
1,2,5	10304.69	17.78	0,0,7	10659.32	−10.24			

Table 4.6: Observed odd symmetry vibrational term values [58] and observed minus calculated values /cm^{-1} for levels above 10,000 cm^{-1}. There are problems with assigning the levels correctly and it is unlikely that all the levels in the table are correctly assigned.

Level 0,0,0			Level 0,1,0			Level 1,0,0			Level 0,2,0			Level 0,0,1		
	Obs	O−C		Obs	O−C		Obs	O−C		Obs	O−C		Obs	O−C
0_{00}	0.0	0.0	0_{00}	749.65	−0.24	0_{00}	1319.79	−1.84	0_{00}	1498.34	−1.84	0_{00}	1616.85	−1.84
1_{11}	8.41	−0.11	1_{11}	8.78	−0.01	1_{11}	8.50	−0.13	1_{11}	9.18	−0.13	1_{01}	0.84	−0.13
2_{02}	2.53	−0.03	2_{02}	2.53	−0.03	2_{02}	2.52	−0.02	2_{02}	2.53	−0.02	1_{10}	8.20	−0.13
2_{11}	10.15	−0.06	2_{11}	10.52	0.06	2_{11}	10.92	0.62	2_{11}	10.92	0.62	2_{12}	9.83	−0.02
2_{20}	32.81	−0.42	2_{20}	34.29	0.04	2_{20}	33.17	−0.52	2_{20}	35.89	−0.52	2_{21}	31.90	0.62
3_{13}	12.57	−0.15	3_{13}	12.94	−0.04	3_{13}	12.64	−0.17	3_{13}	13.33	−0.17	3_{03}	5.03	−0.52
3_{22}	35.34	−0.45	3_{22}	36.81	0.01	3_{22}	35.69	−0.55	3_{22}	38.42	−0.55	3_{12}	12.45	−0.17
3_{31}	73.07	−0.94	3_{31}	76.36	0.09	3_{31}	73.88	−1.16	3_{31}	79.94	−1.16	3_{21}	34.41	−0.55
4_{04}	8.44	−0.09	4_{04}	8.43	−0.10	4_{04}	8.39	−0.08	4_{04}	8.42	−0.08	3_{30}	71.02	−1.16
4_{13}	16.14	0.04	4_{13}	16.50	0.16	4_{13}	16.18	0.03	4_{13}	16.90	0.03	4_{23}	37.77	−0.08
4_{22}	38.72	−0.49	4_{22}	40.19	−0.03	4_{22}	39.05	−0.58	4_{22}	41.79	−0.58	4_{32}	74.38	0.03
4_{31}	76.45	−0.98	4_{31}	79.74	0.05	4_{31}	77.24	−1.20	4_{31}	83.31	−1.20	4_{41}	125.43	−0.58
4_{40}	129.06	−1.67	4_{40}	134.82	0.15	4_{40}	130.47	−2.06	5_{24}	46.00	−0.62	5_{05}	12.58	−1.20
5_{15}	20.07	−0.24	5_{15}	20.42	−0.13	5_{15}	20.08	−0.24	5_{33}	87.52	−1.24	5_{14}	41.96	−2.06
5_{24}	42.94	−0.54	5_{24}	44.41	−0.09	5_{24}	43.24	−0.62	5_{51}	219.08	−2.10	5_{23}	78.58	−0.24
5_{33}	80.68	−1.02	5_{33}	83.95	−0.00	5_{33}	81.43	−1.24				5_{32}	129.63	−0.62
5_{42}	133.23	−1.76	5_{42}	139.04	0.09	5_{42}	134.67	−2.10				5_{41}	194.92	−2.10
5_{51}	200.55	−2.59	5_{51}	209.41	0.20									

Table 4.7: Rotational term values /cm^{-1} and observed minus calculated for new NO_2 potential

Bibliography

[1] M. Born and J. R. Oppenheimer, Ann. d. Phys **84**, 457 (1927).

[2] J. E B Wilson, J. C. Decius, and P. C. Cross, *Molecular Vibrations: The Theory of Infrared and Raman Vibrational Spectra* (Dover, New York, 1980).

[3] C. H. Townes and A. L. Schawlow, *Microwave Spectroscopy* (McGraw-Hill, New York, 1955).

[4] A. R. Hoy, I. M. Mills, and G. Strey, Mol. Phys. **24**, 1265 (1972).

[5] J. K. G. Watson, in *Vibrational Spectra and Structure*, edited by J. R. Durig (Elsevier, Amsterdam, 1977), Vol. 6, ch. 1.

[6] B. T. Sutcliffe and J. Tennyson, Int. J. Quantum Chem. **39**, 183 (1991).

[7] B. T. Sutcliffe, in *Methods in Computational Chemistry*, edited by S. Wilson (Plenum, New York, 1992), Vol. 5.

[8] Lord Rayleigh, *Theory of Sound* (Macmillan, London, 1937), Vol. 1.

[9] W. Ritz, J. Reine Angew Math. **135**, 1 (1908).

[10] B. H. Bransden and C. J. Joachain, *Physics of Atoms and Molecules* (Longman, London and New York, 1983).

[11] R. J. Whitehead and N. C. Handy, J. Mol. Spec. **55**, 356 (1975).

[12] J. Tennyson and B. T. Sutcliffe, J. Chem. Phys. **77**, 4061 (1982).

[13] A. H. Stoud and D. Secrest, *Gaussian Quadrature Formulas* (Prentice-Hall, London, 1966).

[14] C.-L. Chen, B. Maessen, and M. Wolfsberg, J. Chem. Phys. **83**, 1795 (1985).

[15] J. Tennyson and B. T. Sutcliffe, Mol. Phys. **58**, 1067 (1986).

[16] D. O. Harris, G. O. Engerholm, and W. Gwinn, J. Chem. Phys. **43**, 1515 (1965).

[17] Z. Bačić and J. C. Light, Annu. Rev. Phys. Chem. **40**, 469 (1989).

[18] J. C. Light, R. M. Whitnell, T. J. Pack, and S. E. Choi, in *Supercomputer Algorithms for Reactivity, Dynamics and Kinetics of Small Molecules*, edited by A. Lagana (Kluwer, Dordrecht, 1989), Vol. 277, p. 187, nATO ASI series C.

[19] J. R. Henderson, S. Miller, and J. Tennyson, J. Chem. Soc., Faraday. Trans. **86**, 1963 (1990).

[20] C. B. Ludwig, Applied Optics **10**, 1057 (1971).

[21] H. R. A. Jones, A. J. Longmore, F. Allard, and P. H. Hauschildt, Mon. Not. R. Astron. Soc. **280**, 77 (1996).

[22] D. R. Alexander, G. C. Augason, and H. R. Johnson, Astrophysical J. **345**, 1014 (1989).

[23] B. Plez, J. M. Brett, and A. Nordlund, Astronomy and Astrophysics **256**, 551 (1992).

[24] J. M. Brett and B. Plez, Publ. Atron. Soc. Austr. **10**, 250 (1993).

[25] M. S. Bessell and G. S. Stringfellow, Astron. Astrophys. Rev. **31**, 433 (1993).

[26] A. Yoshida and T. Kunimoto, Bulletin Japan Soc. Mech. Engineers **26**, 1929 (1983).

[27] M. C. Fowler, AIAA Journal **19**, 1009 (1981).

[28] W. J. Phillips, J. Quant. Spectrosc. Rad. Transf. **43**, 13 (1990).

[29] C. B. Ludwig, C. C. Ferriso, W. Malkmus, and F. P. Boynton, J. Quant. Spectrosc. Rad. Transf. **5**, 697 (1965).

[30] C. C. Ferriso, C. B, Ludwig, and A. L. Thomson, J. Quant. Spectrosc. Rad. Transf. **6**, 241 (1966).

[31] L. S. Rothman, R. R. Gamache, R. H. Tipping, C. P. Rinsland, M. A. H. Smith, D. C. Benner, V. M. Devi, J.-M. Flaud, C. Camy-Peyret, A. Perrin, A. Goldman, S. T. Massie, L. R. Brown, and R. A. Toth, J. Quant. Spectrosc. Rad. Transf. **48**, 469 (1992).

[32] S. Miller, J. Tennyson, and J. A. Fernley, Revista Mexicana de Astronomia y Astrofisica **23**, 63 (1992).

[33] F. Allard, P. H. Hauschildt, S. Miller, and J. Tennyson, Astrophys. J. **426**, L39 (1994).

[34] J. Tennyson, S. Miller, and C. R. Le Sueur, Comput. Phys. Commun. **75**, 339 (1993).

[35] J. A. Fernley, S. Miller, and J. Tennyson, J. Mol. Spec. **150**, 597 (1991).

[36] P. Jensen, J. Mol. Spec. **133**, 438 (1989).

[37] A. E. Lynas-Gray, S. Miller, and J. Tennyson, J. Mol. Spec. **169**, 458 (1995).

[38] J. Tennyson, J. R. Henderson, and N. G. Fulton, Comput. Phys. Commun. **86**, 175 (1995).

[39] R. B. Wattson and L. S. Rothman, J. Quant. Spectrosc. Rad. Transf. **48**, 763 (1992).

[40] C. D. Paulse and J. Tennyson, J. Mol. Spec. **168**, 313 (1994).

[41] S. Miller, J. Tennyson, H. R. A. Jones, and A. J. Longmore, in *146$^{\rm th}$ I.A.U. Colloquium on 'Molecular Opacities in the Stellar Environment*, edited by P. Thejll and U. Jørgenson (Springer-Verlag, Berlin, 1994), pp. 296–309.

[42] S. Miller, J. Tennyson, and B. T. Sutcliffe, Mol. Phys. **66**, 429 (1989).

[43] P. F. Bernath, *Spectra of Atoms and Molecules* (Oxford, New York, 1995).

[44] K. S. Sidhu, S. Miller, and J. Tennyson, Astron. Astrophys. **255**, 453 (1992).

[45] M. Palao, 1994, final Year Project Report, University College London.

[46] A. J. Sauval and J. B. Tatum, Astrophys. J. Suppl. **56**, 193 (1984).

[47] A. W. Irwin, Astron. Astrophys. **74**, 145 (1988).

[48] T. Yamanouchi and M. Tanaka, J. Quant. Spectrosc. Rad. Transf. **34**, 463 (1985).

[49] P. Jensen, S. A. Tashkun, and V. G. Tyuterev, J. Mol. Spec. **168**, 271 (1994).

[50] O. L. Polyansky, P. Jensen, and J. Tennyson, J. Chem. Phys. **105**, 6490 (1996).

[51] S. Viti, Ph.D. thesis, University of London, 1997.

[52] H. R. A. Jones, A. J. Longmore, F. Allard, P. H. Hauschildt, S. Miller, and J. Tennyson, Mon. Not. R. Astron. Soc. **277**, 767 (1995).

[53] L. S. Rothman, R. Gamache, J. W. Schroeder, A. McCann, and R. B. Wattson, SPIE Proc. **2471**, 105 (1995).

[54] L. S. Rothman, 1996, private communication.

[55] H. Partridge and D. W. Schwenke, J. Chem. Phys. **106**, 4618 (1997).

[56] H. Worden, R. Beer, and C. P. Rinsland, J. Geophys. Res. **102**, 1287 (1997).

[57] J. H. Schryber, S. Miller, and J. Tennyson, J. Quant. Spectrosc. Rad. Transf. **53**, 373 (1995).

[58] A. Delon and R. Jost, J. Chem. Phys. **95**, 5686 (1991).

[59] T. Zimmermann, H. Köppel, and L. S. Cederbaum, J. Chem. Phys. **91**, 3934 (1989).

[60] A. Delon, R. Georges, and R. Jost, J. Chem. Phys. **103**, 1732 (1991).

[61] A. Perrin, C. Camy-Peyret, and J.-M. Flaud, J. Quant. Spectrosc. Rad. Transf. **48**, 645 (1992).

[62] G. Hirsch, R. J. Buenker, and C. Petrongolo, Mol. Phys. **73**, 1085 (1991).

[63] G. Hirsch, R. J. Buenker, and C. Petrongolo, Mol. Phys. **70**, 835 (1990).

[64] G. Hirsch, R. J. Buenker, and C. Petrongolo, Mol. Phys. **73**, 1085 (1991).

[65] G. Hirsch, R. J. Buenker, and C. Petrongolo, Mol. Phys. **76**, 1261 (1992).

[66] E. Leonardi, C. Petrongolo, V. Keshari, G. Hirsch, and R. J. Buenker, Mol. Phys. **82**, 552 (1994).

[67] E. Leonardi, C. Petrongolo, G. Hirsch, and R. J. Buenker, J. Chem. Phys. **105**, 9051 (1996).

[68] S. A. Tashkun and P. Jensen, J. Mol. Spec. **165**, 173 (1994).

[69] P. Jensen, J. Mol. Spec. **128**, 478 (1988).

[70] I. N. Kozin, private communication quoted in referrence [68].

[71] D. Xie and G. Yan, Mol. Phys. **88**, 1349 (1996).

[72] D. Xie and G. Yan, Chem. Phys. Lett. **248**, 409 (1996).

[73] J. H. Schryber, O. L. Polyansky, P. Jensen, and J. Tennyson, J. Mol. Spec. **185**, 234 (1997).

[74] H. Vilanove and M. Jacon, Int. J. Quantum Chem. **55**, 419 (1995).

[75] W. C. Bowman and F. C. De Lucia, J. Chem. Phys. **77**, 92 (1982).

[76] Y. Morino, M. Tanimoto, S. Saito, E. Hirota, R. Awata, and T. Tanaka, J. Mol. Spec. **98**, 331 (1983).

[77] J. Tennyson and B. T. Sutcliffe, Int. J. Quantum Chem. **42**, 941 (1992).

[78] O. L. Polyansky, P. Jensen, and J. Tennyson, J. Chem. Phys. **101**, 7651 (1994).

[79] M. M. Law and J. M. Hutson, Comput. Phys. Commun. **102**, 252 (1997).

[80] P. R. Bevington, *Data Reduction and Error Analysis* (McGraw-Hill, London, 1969).

[81] C. L. Lawson and R. J. Hanson, *Solving Least Squares Problems* (Prentice-Hall, New Jersey, 1974).